THESIS

IMPACT OF THE BOREAL SUMMER INTRASEASONAL OSCILLATION ON THE DIURNAL CYCLE OF PRECIPITATION IN THE ISLAND OF LUZON

Submitted by

Kyle Chudler

Department of Atmospheric Science

In partial fulfillment of the requirements

For the Degree of Master of Science

Colorado State University

Fort Collins, Colorado

Spring 2019

Master's Committee:

Advisor: Steven Rutledge

Weixin Xu
Michael Bell
Steven Reising

ABSTRACT

IMPACT OF THE BOREAL SUMMER INTRASEASONAL OSCILLATION ON THE DIURNAL CYCLE OF PRECIPITATION IN THE ISLAND OF LUZON

The Asian Summer Monsoon (ASM) is a major component of the global weather system with impacts on multiple scales. Driven by the thermal contrast between the Asian continent and the Indian and Pacific Oceans, the monsoon winds bring warm, moist air into the south Asian and maritime continents. Along with this influx of tropical air often comes copious amounts of rain, which can be both beneficial to agriculture and devastating to flood-prone regions. On a larger scale, the immense amount of latent heat released into the upper troposphere from condensation and deposition of water vapor can impact weather patterns across the globe.

One striking feature in rainfall climatology of the ASM is the precipitation maxima located off the western shores of the Western Ghats, Myanmar, and the Philippines. These locations all feature elevated terrain features along their western shores. Many studies have examined why, when monsoon winds impinge upon these mountains, the precipitation preferentially falls off-shore, rather than directly over the mountains where orographic enhancement is strongest. Several theories have been proposed, including convergence of the monsoon winds with a land breeze, afternoon land-based convection which either propagates off-shore or creates a cold pool, and generation of off-shore instability through propagation of gravity waves generated from daytime heating of the boundary layer. Notably, all of these mechanisms are closely tied to the diurnal cycle.

The main source of intraseasonal variability during the summer months in the ASM region is the Boreal Summer Intraseasonal Oscillation (BSISO). Characterized by a broad region of convection which propagates SW to NE from the Indian Ocean to the West Pacific, the BSISO brings alternating 2-3-week periods of inactive and active weather conditions to the monsoon region. Inactive periods are characterized by relatively clear skies, weaker winds, and localized but more intense convection over land. Active periods bring an increase in strong low-level monsoon winds and frequent, widespread precipitation and cloud cover.

In this study, the impact of the BSISO on the occurrence of off-shore precipitation around the island of Luzon is examined. Satellite precipitation estimates show that off-shore precipitation occurs much more frequently during active BSISO phases. Importantly, results also show that a clear diurnal cycle still exists over land during these phases, despite increased cloud cover and reduced solar heating/instability generation. It is hypothesized that the interaction between strong low-level monsoon winds and the diurnal cycle over land is what promotes off-shore precipitation, either through the generation of wind shear (which supports off-shore propagation), or convergence between these winds and a cold pool or land breeze. The stronger low-level winds also cause greater ocean surface energy fluxes, which further promote precipitation. During inactive phases, despite the stronger diurnal cycle over land, the lack of a strong low-level wind results in an environment less conducive to off-shore rainfall.

ACKNOWLEDGEMENTS

I would firstly like to thank my advisor, Dr. Steven Rutledge, for bringing me into the radar meteorology group at Colorado State University, and for his guidance and support throughout this project. Dr. Weixin Xu also deserves a great deal of credit for often being my primary point of contact for assistance in this research endeavor, as well as his initial studies on this topic which my work dovetailed off of. The expertise and direction provided by these two were vital to my progress. I would also like to thank my other committee members, Dr. Michael Bell and Dr. Steven Reising, for their contributions to this thesis.

The rest of the Rutledge research group, Dr. Brenda Dolan, Dr. Brody Fuchs, Karly Reimel, Julie Barnum, Trent Davis, Joe Messina, Adam Clayton, and Marqi Rocque, should also be thanked. I believe the supportive and collaborative environment present within the group is invaluable to successful research. Special thanks to Paul Hein, for his technical support and assistance obtaining the datasets used in this project.

Thanks to the entire crew, science-team and otherwise, of the R/V Thomas G. Thompson for making the 2018 PISTON field campaign such a valuable experience. The many unexpected set-backs and pivots in this project were made up for by being in such good company. Particular thanks to Dr. Timothy Lang, who served as a mentor to me in operating the SEAPOL weather radar on-board the ship. Dr. Lang also provided the idea and guidance for creating the diurnal wind harmonic analysis done in this research.

A great deal of gratitude is also extended towards my friends and family, without whom I certainly would not have kept my sanity though some of the more trying times in working toward this degree. My roommates warrant specific acknowledgements for their support: Michael Natoli

for taking me along on hikes to various epic mountain vistas; and Michael Cheeseman for the stream-of-consciousness dialogues in which we have engaged, which are less accurately described as “conversations” and more aptly described as “therapeutic ramblings”. Finally, a thanks to the City of Fort Collins as whole. I’ve never felt more at home in a city, and I hope to stay here a while longer.

This research is funded by the Office of Naval Research Grant #N00014-16-1-3092.

TABLE OF CONTENTS

LIST OF FIGURES

LIST OF TABLES

CHAPTER 1: INTRODUCTION

1.1 ASIAN SUMMER MONSOON

1.1.1 Overview

The Asian Summer Monsoon (ASM) is a complex system with impacts on multiple scales. Very broadly speaking, the ASM is a period in the boreal summer months where persistent southwesterly winds bring warm, moisture-laden air and precipitation to the continental and island landmasses in eastern and southern Asia, in addition to adjacent ocean waters. In its essence, it is ultimately driven by differential heating rate between land and ocean, with ocean waters having a higher heat capacity than land does (Flohn 1957; He et al. 1987; Li and Yanai 1996; Fasullo and Webster 2003; Ding and Chan 2005), thereby heating the land masses relative to the surrounding ocean waters. This thermal contrast generates a meridional geopotential height gradient, which drives a circulation from ocean towards land. It is essentially the canonical diurnal land-sea breeze concept manifested on a much larger spatial and temporal time scale. This circulation typically begins sometime in May in the Bay of Bengal (BoB) and South China Sea (SCS) and subsequently expands northward. This circulation brings in warm, moist air from the equatorial Pacific and leads to prolonged rainy periods. Fu and Fletcher (1985) showed a high degree of correlation between the interannual variability of rainfall over southeast Asia and the land/sea thermal contrast in the region, supporting the theory that it is this thermal contrast that drives the monsoonal wind and rainfall patterns.

The immense amount of latent heat released by the ASM via condensation and deposition of water vapor has been shown to impact weather patterns on a global scale. Convective activity over the SCS and Philippines has been shown to generate a stationary wave train, which may

impact the location of the downstream subtropical high over the western Pacific (Nitta 1986; Huang and Li 1988; Wang and Ding 1992). Anomalously high monsoon rainfall in India has been shown to correlated with higher rainfall in Northern China and Southern Japan (Kripalani and Kulkarni 1997, 2001). Wang et al. (2001) showed that ASM can produce a meridional tri-polar wave train across the North Pacific, and an anomalous high pressure over Australia.

Within the ASM there exists a complex system of positive and negative feedbacks on multiple spatial scales. Warm tropical sea surface temperatures (SSTs) drive convection through enhanced surface heat and moisture fluxes (Bjerknes 1966). Various studies have found that variation in SSTs over the Indo-Pacific warm pool and monsoon rainfall are well-correlated (Lau and Wu 2001; Pillai and Annamalai 2012). However, as this monsoonal convection becomes more widespread, the enhanced cloudiness may reduce incoming solar radiation, which can lower SSTs (Lau et al. 1997). Rainfall also deposits cooler water onto the ocean surface, further reducing SSTs. When rainfall occurs from isolated convective cells, freshwater sits on the ocean surface in the form of freshwater lenses, which are transient in nature and relatively shallow (Wijesekera et al. 1999; Drushka et al. 2016). Freshwater lenses are of secondary importance to decreased solar radiation in reducing SSTs, but may be locally important in generating circulations that can generate new convective rainfall. Gusty winds associated with precipitation can also lower SSTs through enhanced surface fluxes and mixing cooler water from below to the ocean's surface. However, strong winds occurring over warm SSTs increase sensible and latent heat fluxes to the atmosphere, as the winds allow for a faster rate of heat exchange to the atmosphere (Emanuel 1986). On a more localized scale, impingement of the monsoon westerlies on mountainous terrain features can generate locally heavy precipitation (Smith 1980; Chang et al. 2005; Wang and Chang 2012).

1.1.2 Off-shore Maximum

Figure 1.1 shows the average monthly rainfall across the monsoon region. Values of over 300 mm (~1 ft) per month are widespread, demonstrating the copious amount of moisture the monsoon system generates. In addition to this, one other feature stands out. There is a clear precipitation maximum just off the western edge of many of the landmasses that experience the ASM. West of the Western Ghats of India (Krishnamurti et al. 1983; Grossman and Durran 1984), the western shore of Myanmar in the BoB (Zuidema 2003; Xie et al. 2006), and the west coast of the Philippines in the SCS (Ho et al. 2008) all show this pronounced off-shore maximum. These locations all coincide with coastal elevated terrain features which extend essentially perpendicular to the monsoonal flow (Figure 1.2). It seems clear then that orography is likely contributing to these maxima in some manner. However, if it was purely upslope flow causing the precipitation, one would expect the maxima to be near the peaks of mountain ranges, as opposed to displaced to the western side, over water in fact.

These off-shore rainfall maxima have been examined in numerous modeling studies. Ogura and Yoshizaki (1998) utilized a two-dimensional cloud model to examine the W. Ghats precipitation maximum. They found that both vertical wind shear and ocean surface fluxes were important for capturing the off-shore precipitation in their model simulations. When ocean fluxes were suppressed, the precipitation maximum shifted to the mountainous area. Furthermore, when a uniform vertical wind profile was used, the rainfall was about half that observed. Only by including both a typical monsoonal wind profile (westerlies in the low-levels, easterlies aloft) and ocean surface fluxes did the model correctly simulate the off-shore maximum. Xie et al. (2006) found that even the relatively small and narrow mountain ranges of Myanmar cause enough impedance of the monsoon flow to create the convergence necessary to generate convection. They

found that simulating orographic convection in their atmospheric model not only had impacts specific to the mountain ranges, but also had significant impacts on strengthening the hydrological cycle across the entire monsoon region.

While these modeling studies highlight the importance of these off-shore precipitation maxima and outline some possible large-scale mechanisms, they do not account for the diurnal cycle of precipitation at the coast. Several past field projects have shown that the diurnal cycle is a crucial element to explaining coastal rainfall. In the Winter Monsoon Experiment (WMONEX, Houze et al. 1981), the land/sea breeze cycle was determined to be a key component to the observed off-shore rain. The nighttime land breeze was shown to converge with the low-level monsoon flow to produce lift and precipitation offshore. In the Terrain-Influenced Monsoon Rainfall Experiment, (TiMREX) Ruppert et al. (2013) found that katabatic drainage winds from the mountain ranges further enhanced off-shore flow and therefore convergence with the westerlies. And in the North American Monsoon Experiment (NAME, Nesbitt et al. 2008; Lang et al. 2007), off-shore propagation was determined to contribute a significant fraction of the off-shore precipitation. Afternoon convection formed over the Sierra Madre Occidental, and then propagated westward as an organized mesoscale convective system into the Gulf of California. Finally, Mapes et al. (2003) proposed a gravity wave mechanism for off-shore rainfall adjacent to land masses. They argued that daytime heating over the land expands the boundary layer, causing gravity waves to propagate away from the disturbed region. These gravity waves act to destabilize the air over the neighboring waters, thereby generating convection. It is also plausible that all of these mechanisms may work in tandem to produce the off-shore precipitation maxima observed.

1.2 INTRASEASONAL VARIABILITY

1.2.1 Active/Inactive Periods

After the onset of the ASM, a typical season will be punctuated by alternating inactive and active periods (inactive periods are also referred to as "break" or "suppressed" periods in other literature). The difference between these two convective regimes has been covered in many studies (e.g. Williams et al. 1992; Petersen and Rutledge 2001; Xu and Zipser 2012). Active periods are characterized by widespread, moderate precipitation rates (Xu and Zipser 2012), and significant warm-rain processes (Petersen and Rutledge 2001; Xu and Zipser 2012). In an inactive period, clearer skies lead to deeper instability and more intense storms (Ho et al. 2008; Xu and Zipser 2012), with ice-based precipitation via riming. Consequently, lightning activity is also much greater during inactive monsoon periods (Petersen and Rutledge 2001). Looking specifically at the SCS, Ho et al. (2008) found that inactive phase precipitation tended to be more land-based. During inactive phases when cloud shading is less persistent, radiative heating over land can generate greater instability and more intense storms. Aerosol loading may also play a role in invigorating storms over land (Rosenfeld and Lensky 1998; Williams and Stanfill 2002; Lau and Kim 2006). However, the SCS is surrounded by many significant aerosol sources, and it is possible that there is some aerosol effect even over the open ocean.

1.2.2 The Boreal Summer Intraseasonal Oscillation

The inactive and active periods of the ASM can be more broadly examined through the scope of the Boreal Summer Intraseasonal Oscillation (BSISO). A warm-season analog to the wintertime Madden Julian Oscillation (MJO), the BSISO consists of a convective envelope propagating from the Indian Ocean to the West Pacific (BSISO1, Wang and Xie 1997; Lee et al. 2013). In addition to the eastward propagating component seen in the MJO, the monsoon wind

profile causes the BSISO to also have a northward propagation. Figure 1.3, adapted from Lee et al. 2013 (described in further detail in Chapter 2), shows this propagation in the frame of outgoing longwave radiation (OLR) anomalies. A northwest-to-southeast aligned band of negative OLR anomalies propagates from the BoB to the SCS. Associated with these negative OLR anomalies are positive precipitation anomalies and increased southwesterly monsoon flow. A full BSISO oscillation takes approximately 30-60 days. There is also a 10-20-day mode of the BSISO (BSISO2, Wang 2005; Lee et al. 2013), associated with a southwest-northeast frontal rainband, however this mode will not be considered in this study.

Recently, extensive work has been done in investigating the BSISO and its relation to the ASM. Kang et al. (1999) found that the East Asian rainband associated with BSISO2 was crucial to developing the subtropical monsoon gyre and initiating the ASM. Hsu et al. (2016) showed that phases 2-4 of BSISO1 and phases 5-7 of BSISO2 were linked to a 50% increase in the likelihood of extreme rainfall events in Southern China. Expanding the analysis across the ASM region, Lee at al. (2017) found that when the BSISO positive precipitation anomaly reaches a given area, the probability of an extreme precipitation event increases from 10% to 40-50%. Chen and Zhai (2017) examined temperature anomalies and found that phases 2-4 of BSISO1 brought a fivefold increase in the likelihood of extreme high temperatures in Southeast China. Mesoscale details can also be influenced by the BSISO. In the BoB, instability, convective organization and size, and lightning activity were all shown to be related to BSISO1 phase by Virts and Houze (2016). They found that during active periods, the Bay of BoB had more frequent occurrences of large, organized mesoscale convective systems (MCS) and subsequently greater rainfall. Active periods were also shown to have more lightning over the BoB, although this lightning was not collocated with the MCS's. The BSISO also can influence weather and climate on a hemispheric scale by altering the

midlatitude circulations directly (Ding and Wang 2005) or indirectly influencing the monsoon activity in other parts of the world (West North Pacific Summer Monsoon and North American Summer Monsoon, Moon et al. 2013).

It is easy from here to tie the BSISO back in with the inactive and active monsoon periods (Hoyos and Webster 2007; Ding and Wang 2009). An active monsoon period is associated with a phase of the BSISO which brings cloudiness (negative OLR anomalies), persistent rain (positive precipitation anomalies), and a stronger monsoon flow. The inverse holds for inactive monsoon periods. From this, one can relate a phase of the BSISO to an active/inactive period at a given location. Specifically looking at the Philippines, Figure 1.3 shows that phases 1-3 of the BSISO can be considered inactive, and phases 5-7 are in the active phase. These definitions are what will be used for the rest of this study, when referring to inactive or active periods.

Xu and Rutledge (2018) performed an extensive study on the variability of convection in relation to the BSISO in the SCS and Philippines region. Their findings are summarized in Figure 1.4. During active phases, precipitation systems were generally larger in size and contained a larger stratiform fraction, possibly due to higher shear and moister midlevels. Instability was found to be higher over the Philippines during inactive periods compared to active periods. The opposite relation was found over the SCS, although it was found to have only a small impact on convective intensity over the SCS. The cloud population over the SCS during inactive phases was found to have a trimodal distribution between shallow cumulus, congestus, and deep convection, as is commonly seen in the tropical open ocean regions (Johnson et al. 1999). During active phases, the shallow cumulus population was reduced. Finally, during inactive phases, a strong contrast in convective systems was noted between land and sea. Intense convection was more frequent over the land compared to the sea, as marked by stronger microwave ice scattering signatures and 30-

dBZ echo top heights which extended further into the mixed-phase region. This is in contrast with active phases, where the difference between land and ocean convection was less apparent. Xu and Rutledge suggested that a reason for this may be the strong diurnal cycle over land during inactive phases, which will be a main focus of this research.

The BSISO is generally poorly predicted by numerical weather models (Waliser et al. 2003; Kim and Kang 2008; Sabeerali et al. 2013). Key aspects such as tropospheric heat and moisture profiles, air-sea surface fluxes, ocean mixing, and other mechanisms are poorly represented by these models and render them unable to fully capture the complexity of the BSISO. A more concrete physical understanding of these factors is the only way to improve model forecasts. The 2019 Propagation of Intraseasonal Oscillations (PISTON) field campaign will seek to provide extensive observations towards this end. Located off the western coast of Luzon in the Philippines, PISTON will provide extensive observations of atmospheric and sea conditions through balloon soundings, oceanographic profilers, a state-of-the-art shipborne polarimetric radar, and other instruments. Note: The PISTON 2018 field campaign was supposed to focus on the land-sea contrast and diurnal cycle over the SCS immediately west of Luzon but approval from the Philippines to operate a U.S. research ship in this area was not granted. Instead PISTON 2018 was conducted east of Luzon in international waters.

1.3 OVERVIEW AND GOALS

The off-shore rainfall maxima observed off the west coast of the W. Ghats, Myanmar, and the Philippines during the ASM are interesting features with significant import to the coastal cities in these regions. Because these regions all have some degree of elevated terrain features along the coast, and monsoon winds flow up these slopes, it stands to reason that orographic lifting plays a

role in generating precipitation. However, the displacement of the maxima to the west of the mountain peaks, over adjacent waters, suggest there are other factors at work.

Modeling studies have suggested that wind-enhanced sea-air surfaces fluxes, vertical wind shear, and impingement of large-scale westerlies on the mountain slopes all play a role in producing the off-shore maximum. However, these modeling studies fail to consider the diurnal cycle, which previous field work has shown to be important (WMONEX, Houze et al. 1981; NAME, Nesbitt et al. 2008; Lang et al. 2007; TiMREX, Ruppert et al. 2013). Possible mechanisms through which the diurnal cycle influences off-shore precipitation include convergence of the monsoon westerlies with a land breeze cycle (Houze et al. 1981), katabatic drainage winds (Ruppert et al. 2013), cold pools from terrain-based convection (Xu et al. 2012), or off-shore propagation of convective systems (Lang et al. 2007, Nesbitt et al. 2008), or instability generated by gravity waves (Mapes et al. 2003).

Many of the mechanisms outlined above rely either on a strong SW monsoonal flow to create convergence along the coast and enhance surface fluxes, or daytime instability over land to generate convection. These two variables are greatly influenced by the phase of the BSISO. Inactive phases bring reduced cloud cover and enhanced surface heating and instability over land, but weaker monsoon winds. The inverse is true for active phases. Other key variables like SST and wind shear are also impacted by the BSISO.

Global-scale models struggle to predict the ASM and BSISO on a seasonal level with much skill (Waliser et al. 2003; Lin et al. 2006; Fu et al. 2007; Kim and Kang 2008; Matsueda and Endo 2011; Sabeerali et al. 2013). These models poorly represent the diurnal cycle of tropical convection, which has been shown to have significant impacts on the entire monsoon system (Yang and Slingo 2001; Dai and Trenberth 2004; Chow and Chan 2009). Improving our understanding

of the diurnal cycle will lead to more accurate predictions of this important weather system. Narrowing in on the Philippines, which will be the region of operation for the 2019 PISTON field campaign, the focus of this study is to examine the interaction between the BSISO and the diurnal cycle of precipitation, and how it relates to the off-shore precipitation maximum observed there.

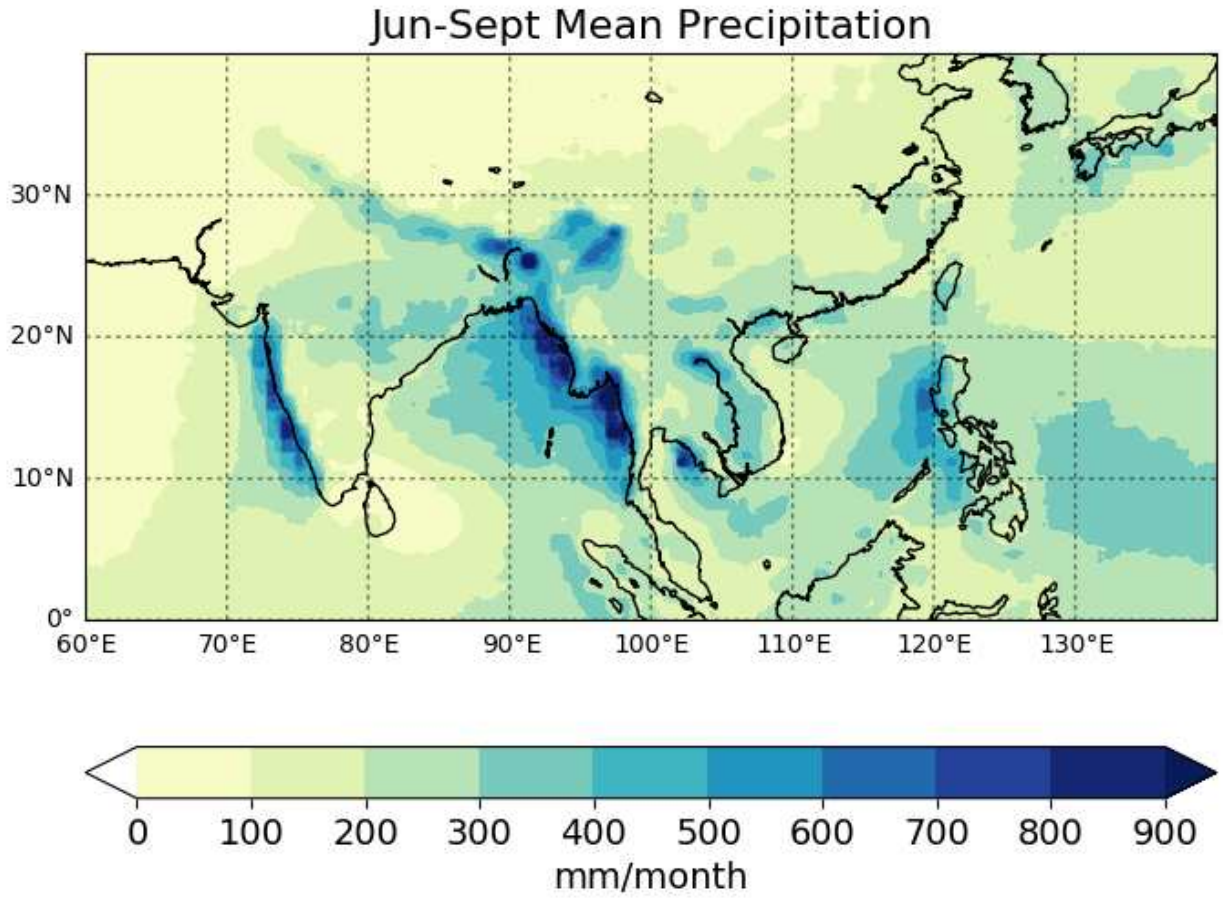

Figure 1.1: Mean monthly precipitation, as measured by the TRMM 3B43 multi-satellite estimate.

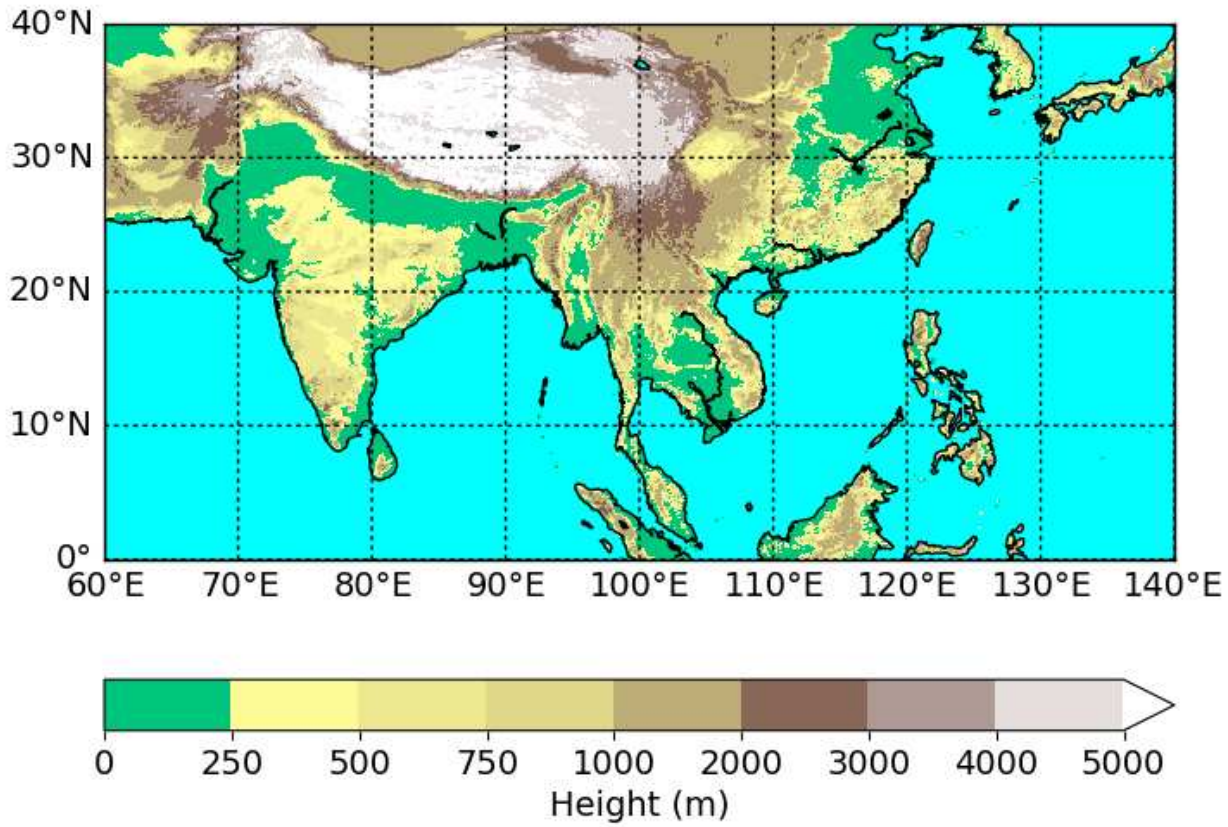

Figure 1.2: Land elevation in the monsoon region. Data from the Shuttle Radar Topography Mission (https://dds.cr.usgs.gov/srtm/)

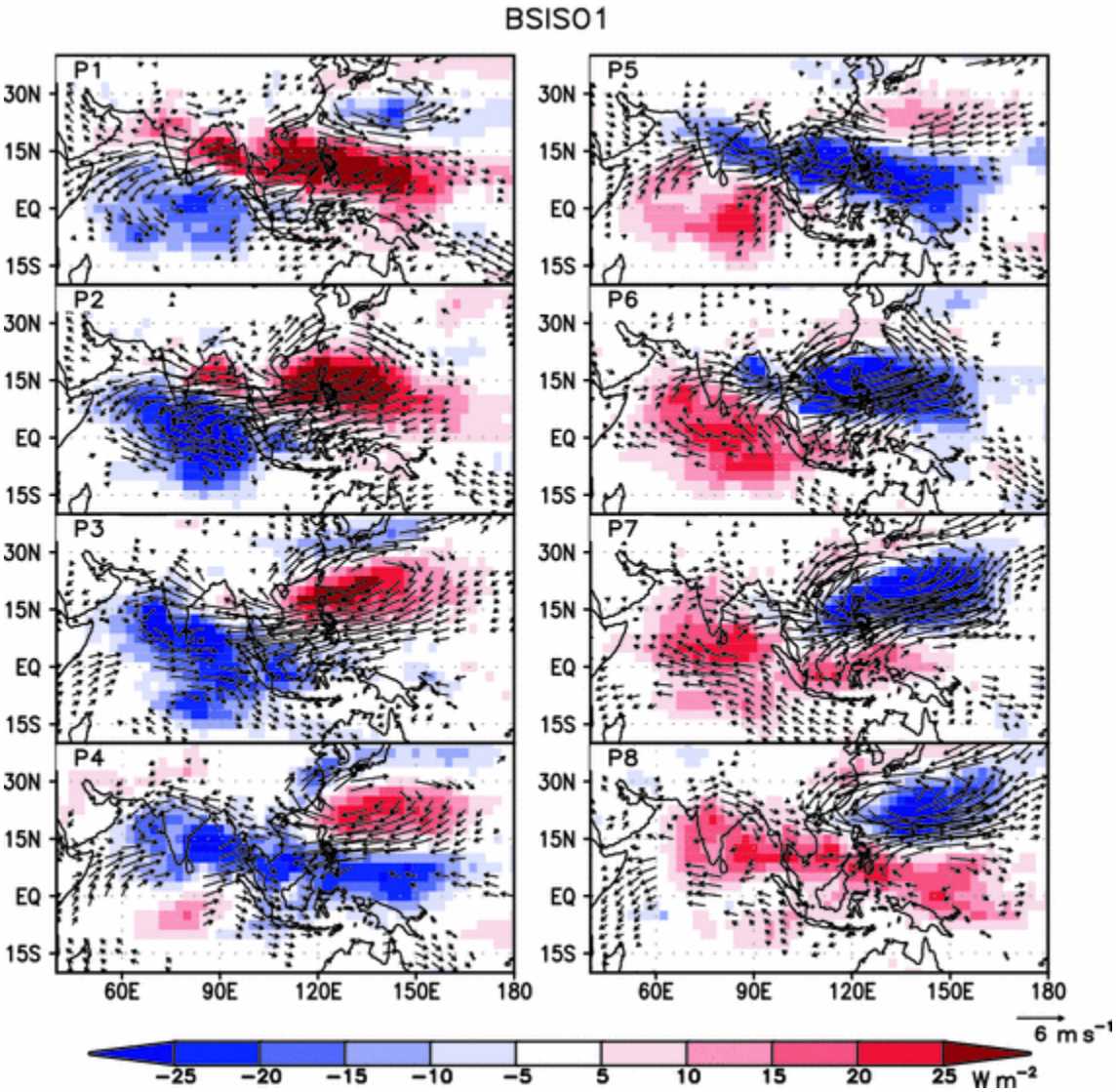

Figure 1.3: Anomalies of OLR (shading) and 850mb wind (vector) for the different BSISO indices. Adapted from Lee et al. 2013)

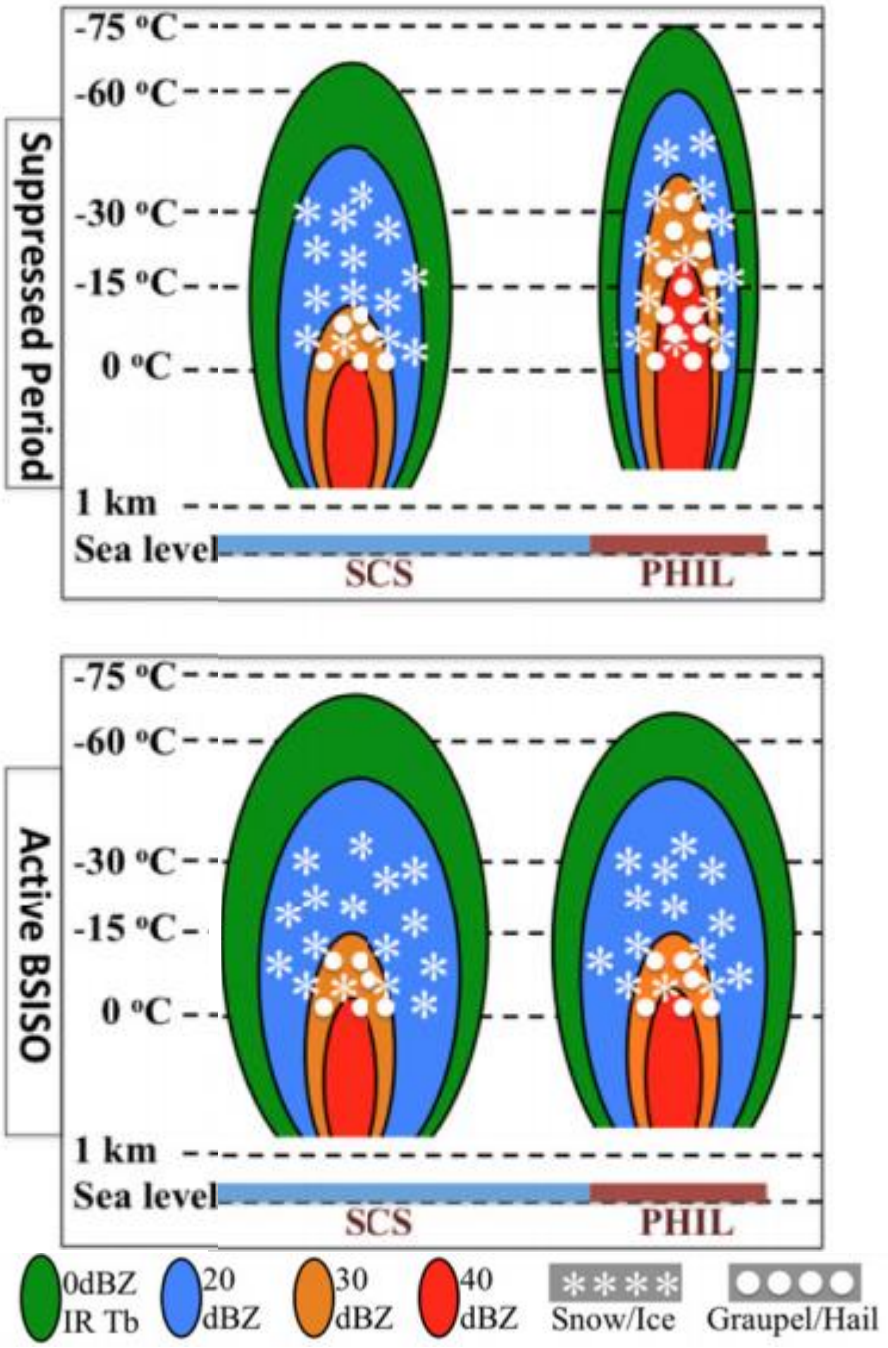

Figure 1.4: Conceptual model of precipitating systems during the boreal summer in the Philippines (PHIL) and South China Sea (SCS). Adapted from Xu and Rutledge 2018.

CHAPTER 2: DATA AND METHODOLOGY

2.1 OVERVIEW

To study the rainfall patterns and diurnal cycle in the SCS, spaceborne radar products from the Tropical Rainfall Measuring Mission (TRMM) and Global Precipitation Measurement mission (GPM) are used. Specifically, the TRMM Precipitation Radar (PR) and GPM Ku-Band (KuPR) radar scans, as well as the TRMM Precipitation Feature (PF) database are used. Data are stratified both by the BSISO Index defined by Lee et al (2013), as well as by wind regime as calculated by the Cross-Calibrated Multi-Platform (CCMP) wind vector analysis product. This study focuses on a region bounded by 10°-20°N and 115°-125°E, which contains the main landmass of the Philippines as well as the surrounding sea (Figure 2.1). Topography information used in this study is from the Shuttle Radar Topography Mission. The European Centre for Medium-Range Weather Forecasts interim reanalysis (ERA-Interim) dataset (Dee et al. 2011) from 1998-2017 was used to examine the climatological values of convective available potential energy (CAPE), vertical wind shear, 500mb heights, 850mb winds, sensible and latent heat fluxes, 2-meter temperature, and solar radiation across different BSISO phases. SST is similarly examined using the NOAA Optimum Interpolation Sea Surface Temperature dataset (Banzon et al. 2016). Only climatological and satellite data from June-September are included in the analysis, which corresponds to periods when the monsoon and BSISO signal are typically strongest. Days where the BSISO amplitude (defined below) was less than 1 were also excluded from the analysis. Finally, days where the BSISO phase was 4 or 8 were not included, as these represent the transition period between the “Inactive” (phase 1-3) and “Active” (phase 5-7) periods. Table 2.1 summarizes the total number of TRMM overpasses, GPM overpasses, and PFs in each BSISO phase.

2.2 TRMM PRECIPITATION FEATURES

This study will utilize the TRMM PF Database to generate statistics on the characteristics of raining systems in the region. As outlined in Liu et al. 2008, the database takes TRMM PR data and groups together surface raining pixels which are contiguous in space. Once a feature is outlined, the location of the PF is determined as the centroid of an ellipse surrounding the raining pixels. In addition to the three-dimensional PR radar data, measurements from other TRMM instruments (Kummerow et al. 1998) such as the Lightning Imaging Sensor (LIS), Visible and Infrared Scanner (VIRS), and Microwave Imager (TMI) can then be collocated with the PF. From this, information such as average rain rate, convective area, reflectivity echo heights, and lightning frequency can be defined for the PF. The date and time the PF was observed is also recorded, which allows for analysis on how these PFs may change in an area over time. Over 33,000 PFs have been compiled and analyzed in the analysis.

2.3 TRMM AND GPM RADAR

The TRMM PF database provides an overview of precipitation frequency, intensity, and morphology. However, although PFs can sometimes be very large and span over both the open ocean and the mountainous terrain in this region, just a single value of rain rate, echo height, lightning rate, etc. are given for an entire PF. Because of this, the distinction between land- and sea- based precipitation can often be blurred when looking at PF statistics. To resolve this issue, high resolution satellite radar scans from the TRMM PR and GPM KuPR are utilized. The Version 7 2A25 and Version 5 2A products were used for TRMM PR and GPM KuPR, respectively, which provide attenuation-corrected vertical profiles of reflectivity and surface rain rate estimates, as well as rain type classification. The GPM Ku-Band radar was chosen over the Ka-Band and matched-scan products for its wider viewing swath and greater spatial coverage. The TRMM PR

has a horizontal resolution of about 5km, and a vertical resolution of 250 meters up to 20km. The GPM KuPR has the same horizontal resolution, and a 125-meter vertical resolution. For the purposes of this research, radar data were interpolated onto a 0.5-degree horizontal grid over the study region. This provides rain rate information on a scale fine enough to resolve the differences between land and sea precipitation. The fine vertical resolution of the radars also allows a detailed analysis of the vertical structure of raining systems in the region. Seventeen years of satellite radar data from TRMM PR (1998-2014) and three years of data from GPM KuPR are gathered, over 6500 overpasses in total.

2.4 RAPIDSCAT WIND MEASUREMNTS AND DIURNAL HARMONIC FITTING

The RapidScat scatterometer is a spaceborne instrument which measures surface wind speed and direction over the ocean. RapidScat (and scatterometers in general) make use of the fact the ocean surface roughness varies with wind speed. By observing the radar backscatter cross-section over the open ocean at several viewing angles, the wind speed and wind direction can be calculated. (Fore et al. 2014). Because RapidScat is affixed to the International Space Station, which is not in a sun-synchronous orbit, it is able to take measurements at a given location at different times each day. This affords the opportunity to study how surface winds change throughout the day.

A diurnal harmonic fitting method (as done in Gille et al. 2005) was performed on the RapidScat data to examine the diurnal cycle of ocean surface winds in Chapter 3.3.1. Wind measurements are first binned up and averaged by location and time of day. At a given grid box, a harmonic (or ellipse) equation is fit to the 3-hourly mean wind measurements using a least-squares method. The fitted equations are

$$u = u_0 + u_1 \cos(\omega t) + u_2 \sin(\omega t) \quad (2.1)$$

$$v = v_0 + v_1 \cos(\omega t) + v_2 \sin(\omega t) \quad (2.2)$$

Where $\omega = 2\pi$ day^{-1}. Where the fit is good and the amplitude is high, a wind regime that is has a strong diurnal forcing is likely to exist. Then, the mean wind at each grid box is subtracted from the diurnal harmonic to get a wind anomaly at each timestep. The direction of this anomaly represents the phase of the rotation that diurnal cycle is in at each time step.

2.5 CCMP WIND RETREIVAL

The BSISO drives changes in wind regimes between inactive and active phases around Luzon. The CCMP wind retrieval product is used to obtain historical gridded wind data over the study region. CCMP utilizes a variational analysis method (VAM) (Atlas et al. 2011) to combine wind measurements from moored buoys and microwave radiometers and scatterometers (ASCAT, QuickScat, SSM/I, SSMIS, AMSR, TMI, WindSat, and GMI) with reanalysis data from ERA-Interim. From this, global 0.25-degree gridded 6-hourly wind vector estimates are produced. The VAM attempts to create a gridded surface wind analysis which minimizes misfit between the analysis and the known background, a priori constraints, and the instrument measurements. CCMP provides the temporal and spatial resolution needed to study the diurnal cycle and land-sea interaction. An average wind speed and direction is determined over the study area for each TRMM/GPM overpass, which is then used to stratify the radar data into different wind regimes. By combining rainfall information from TRMM and GPM with wind estimates from CCMP, a more complete picture is established of the complex diurnal cycle.

2.6 BSISO INDEX

This research will primarily examine the differences in precipitation characteristics between inactive and active BSISO periods. Towards this end, the index defined by Lee et al.

(2013) (hereafter referred to as L13) is used to determine the phase and amplitude of the oscillation at the times of the satellite overpasses. The L13 study performs multivariate empirical orthogonal function (MV-EOF) analysis on a 30-year record of 850hPa zonal (U850) wind and outgoing longwave radiation (OLR) anomalies over the Asian Summer Monsoon region (10°S–40°N, 40°–160°E). Only the summer months (May-October) were examined in their analysis. From these MV-EOFs, the principal components (PCs) of variability are determined. L13 found that the first and second PCs describe the 30-60-day oscillation that is pertinent to this study. The first and second PCs are then combined into a single index, much like the well-established MJO index created by Wheeler and Hendon (2004). On a given day, each PC will have a different "strength", determined by how well they describe the U850 and OLR at that time. The amplitude of the BSISO is defined in this index as $(PC_1^2 + PC_2^2)^{1/2}$, while the phase depends on the relative strength of the PCs. This index is available online at http://iprc.soest.hawaii.edu/users/jylee/bsiso, with daily amplitude and phase values from 1981 up to the present day.

Historical BSISO indices are calculated by first applying a 25-90-day bandpass filter on to the OLR and U850 fields, and then projecting the resulting smoothed field onto the EOF-derived fields in Figure 1.3. One advantage of the Lee et al. index is that real-time indices can be calculated without the needing to apply bandpass filtering to the real-time OLR or U850 data. It is this non-filtered, real-time index that will be utilized for the purposes of this study. The justification for this decision lies in the real-time index's ability to better capture the day-to-day variability in the Luzon region. While the time-filtered index better represents the idea of a broad convective envelope traversing across the region, in reality the transition between phases is likely not always smooth. Day-to-day variability in localized wind patterns and cloud coverage are lost when looking at the time-filtered index. In other words, if a given day has the typical look of an active period (strong

SW flow, high coverage of rain), but it was preceded by a string of inactive days, the smoothed index may not label that particular day as active. For this study, the main interest lies in the how wind flow and cloud coverage associated with typical active/inactive conditions impact precipitation around Luzon on a daily time scale. The smooth progression of single BSISO events across the entire ASM region is not particularly important here. Using the real-time index provides a way to classify individual days as inactive or active, without the influence of other days.

Table 2.1: Number of satellite overpasses and TRMM Precipitation Features (PFs) in each BSISO phase. Only instances where the BSISO amplitude is greater than 1 are included in the totals.

	BSISO Phase							
	1	**2**	**3**	**Inactive Total**	**5**	**6**	**7**	**Active Total**
TRMM	673	877	643	2193	812	594	692	2 098
GPM	65	103	40	208	123	58	76	257
PFs	4648	5410	5044	15 102	7469	5948	4885	18 302

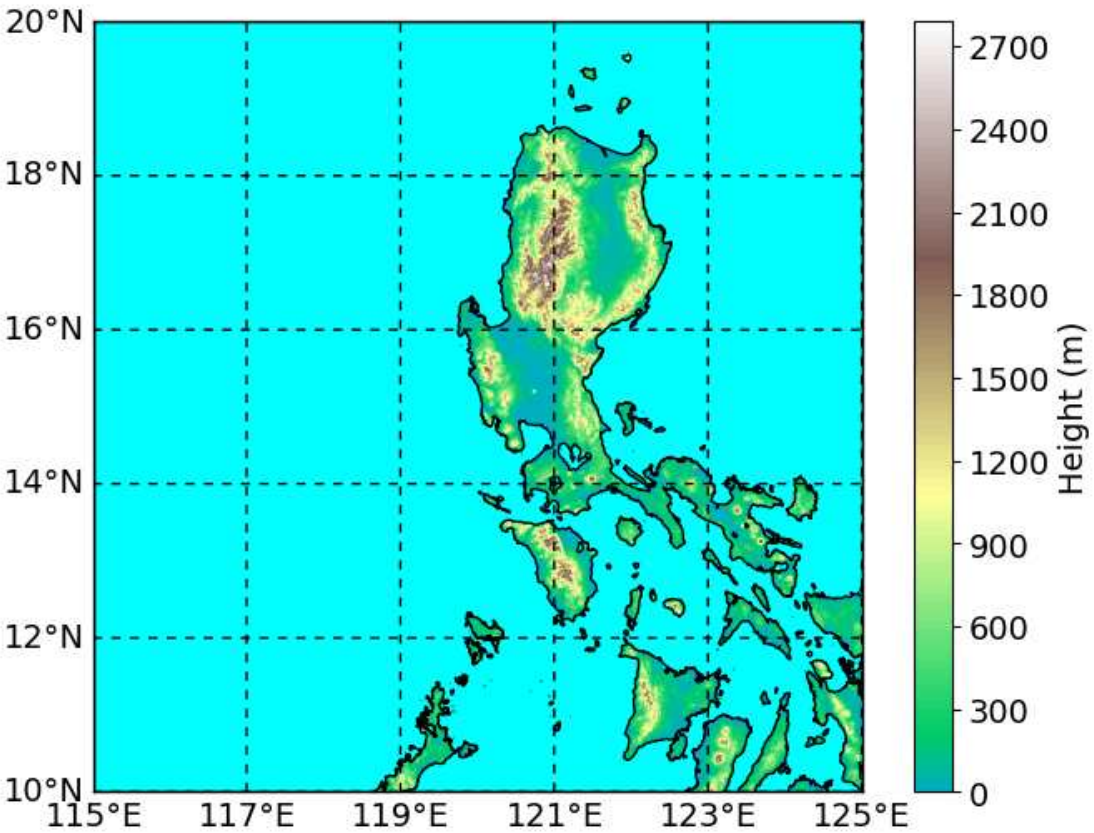

Figure 2.1: Topographic map of the study region

CHAPTER 3: RESULTS

3.1 OVERVIEW

The following sections will analyze the characteristics and location of precipitation over Luzon and the surrounding ocean during different phases of the BSISO. First, environmental conditions associated with each phase will be examined with reanalysis data and surface wind measurements. Rainfall variation between inactive and active phases of the BSISO will also examined. Next, the diurnal cycle will be studied through analysis of scatterometer measurements, PF characteristics, and surface rainfall. Finally, the vertical structure of convective systems in inactive and active phases will be assessed using reflectivity profiles from TRMM PR and GPM KuPR.

3.2 INTRASEASONAL VARIABILITY

3.2.1 Reanalysis Data

Figure 3.1 shows the June-September mean 500mb geopotential heights and 850mb wind vectors during each phase of the BSISO. In inactive phases (phase 1-3), the flow is dominated by the Western Pacific subtropical high to the NE of the study region. Peaking in strength and westward extent during phase 3, this high weakens or even reverses the southwesterly monsoon flow at low levels. This high pressure moves eastward away from the Philippines in phase 4, and in phase 5, a low pressure center forms over the SCS. This marks the beginning of the active phases (5-7) and is accompanied by strong low-level southwesterlies. As this zone of low pressure expands eastward and northward in phases 6 and 7, the monsoon flow strengthens over the region. The strongest winds (12-14 m s^{-1}) are noted in the southern half of the region, where the pressure gradient is larger.

Mean June-September CAPE is shown in Figure 3.2. CAPE was accumulated from the near-surface level (1000mb for over the ocean, 925mb over land) up to the level of neutral buoyancy. Over the land, CAPE is maximized during inactive phases, due to increased solar insolation (Figure 3.7) and subsequent greater surface heating. Over the ocean, however, CAPE is maximized during active phases. Although there is also a reduction in solar heating over the ocean, this is likely counteracted by the increase in sensible and latent heat fluxes from the ocean surface.

The equations for sensible heat (SH) flux and latent heat (LH) flux are

$$SH = C_H U(T_s - T_a) \tag{3.2}$$

$$LH = C_E U(q_s - q_a) \tag{3.1}$$

Where C_H and C_E are transfer coefficients, U is the surface wind speed, T is temperature, q is the specific humidity, and the subscripts s and a represent those variables at the land/ocean surface and 10m height, respectively (Wang et al. 1996). Because 2-meter temperature (Figure 3.4) and SST (which also controls q_s) (Figure 3.3) only change by a less than one degree Celsius between inactive and active phases (about a 2% change), and surface wind speed (Figure 3.11) more than doubles in places, the change in U dominates the changes in SH and LH. Since low level winds are considerably stronger during active phases surface sensible and latent heat fluxes are much greater over the ocean during active phases. This is also seen in the reanalysis data (Figure 3.5, Figure 3.6). Over the land, the inverse is true. Greater solar insolation during inactive phases heats up the land and generates a sharper temperature gradient (higher sensible heat fluxes), and drier boundary layer air promotes greater latent heat fluxes. The frictional wind speed reduction over land also results in the wind-induced flux increase over the ocean is not as strong over the land.

Vertical wind shear across multiple depths was also examined with reanalysis data. Vertical wind shear has been shown to be important to the development and maintenance of

mesoscale convective systems in both numerical models (Thorpe et al. 1982; Moncrieff and Liu 1999; Coniglio et al. 2006; Zheng et al. 2013; Alfaro and Coniglio 2018) and in field project case studies (Lang et al. 2007; Saxen and Rutledge 2000). Thus, higher values of vertical wind shear may aid isolated terrain-based convection in growing upscale and propagating off-shore. Vertical wind shear was found to be higher in active BSISO phases at low-levels (10m – 850mb, Figure 3.10), mid-levels (850 – 500mb, Figure 3.9) and a deep-layer (Figure 3.8 700-150mb). During active phases, strong low-level westerlies (monsoonal flow) are situated below enhanced upper-level easterlies (due to increased divergence aloft), creating increased deep-layer and mid-level shear. At the lowest levels, the direction of the shear vectors is reversed, possibly due to a friction-induced weakening of winds at the 10 m level. The strongest shear is seen in the SW corner of the map, where the monsoonal flow and upper-level easterlies (not shown) are typically the strongest (Figure 3.1).

3.2.2 Surface Winds

Figure 3.11 shows the mean CCMP surface wind vectors during inactive and active phases. Active phases feature strong southwesterly monsoonal flow across most of the domain, especially the southern portions. The flow weakens and turns more northerly as it begins to wrap around the monsoon low in the SCS. In inactive phases, the flow is much weaker and generally southerly or non-directional. Influence of the Western Pacific subtropical high is noted to the east and northeast of Luzon, where the flow has a slight easterly component.

The domain-average surface wind speed and direction was calculated for the CCMP analysis that was closest to each TRMM/DPR overpass and tabulated into histograms (Figures 6-8). For overpasses that occurred during active phases, 74% of the mean wind vectors were from the SW (180-270°) (Figure 3.12). Overpasses during inactive phases were associated with a wider

variation in wind directions, with the mean wind having an easterly component (0-90°) 51% of the time. Examining wind speed (Figure 3.13), overpasses during active phases were associated with surface winds about 3 m s^{-1} stronger on average than during inactive phase overpasses. The distribution of wind speeds during active phases is also wider. A similar pattern is seen when stratifying overpasses by domain-mean wind direction rather than by phase (Figure 3.14). The average wind speed during easterly wind regimes is 2.7 m s^{-1} weaker compared to westerly regimes. This reinforces that inactive regimes are tied to weaker winds with at least somewhat of an easterly component (also seen in Figure 3.11).

3.2.3 Rainfall

Mean surface rain rate from PR (TRMM) and DPR (GPM) was calculated on a 0.5x0.5-degree grid and partitioned by inactive and active periods (Figure 3.15). CCMP surface winds from Figure 3.11 are also shown for added context. The domain-mean rain rate during active phases is more than double that of inactive phases (0.27 vs. 0.57 mm h^{-1}). In inactive phases, a clear precipitation maximum is apparent over the high terrain of Luzon. There is also some evidence of off-shore propagation, with higher rain rate values extending out into the coastal waters around 16-17° N. During active phases, widespread precipitation is noted over all the surrounding ocean, particularly to the west of Luzon. Interestingly, the highest mean rain rate values are observed to the southwest of Luzon. Further north, where the flow turns more northerly (and more in parallel with the coast), the mean precipitation rate is lower. Rainfall also decreases towards the west edge of the map as distance increases from the coast. These two observations suggest that convergence of the monsoon flow with some coastal feature (land breeze, cold pool, etc.) may play a role in generating the off-shore precipitation. It should be mentioned that there is still precipitation over

the mountain peaks in active phases, although the signal is muted in Figure 3.15 due to the stronger off-shore rain signal.

It is possible that anomalously high rain rates observed during a single overpass could throw off the mean rainfall calculated for Figure 3.15. With that in mind, Figure 3.16 simply shows the fraction of satellite overpasses that observed precipitation in each grid box. A grid box was considered to have rain during a given overpass if the radar mapped at least 10 pixels with a rain rate greater than 2 mm h^{-1}. Below this threshold, noisy, spurious raining pixels contaminate the dataset. The tendency of precipitation to preferentially fall on the southwest side of the islands is even more evident here. Locations where the coast runs directly perpendicular to the monsoon flow (Zambales, 120° E 15°N; Mindoro 121° E 13° N) see the heaviest rainfall.

In attempt to isolate the effect of the different wind patterns on precipitation, satellite rainfall data were also stratified by wind regime (Ho et al. 2008 also used wind regime to define inactive and active phases). Each satellite radar overpass was associated with either an easterly or westerly wind regime, as determined by the domain-mean surface wind vector during the closest CCMP analysis time. To try to further capture the effect of wind speed and direction, only instances where the magnitude of the mean vector was greater than 3 m s^{-1} (approximately the median of all overpasses) were considered. New plots of mean rain rate (Figure 3.17) and rain frequency (Figure 3.18) were produced using this method. Like active BSISO phases, westerly wind regimes have frequent precipitation just off the west coast. Compared to the mean active BSISO wind field, the mean westerly-regime wind field has strong southwest winds extending further north. This is possibly due to the inclusion of BSISO phase 8, during which time the monsoon low track shifts northward (Figure 3.1). The result of this is the off-shore precipitation signal extending further

north along the coast, further highlighting the importance of the SW winds in generating coastal rain.

Interestingly, there is also a precipitation maximum to the east of the island (122° E, 15° N) in the easterly wind regime. The east coast of Luzon also features elevated terrain. Although these peaks are about half the height of those on the west coast, relatively small terrain features have still been shown to cause enough speed convergence to create convection (Xie et al. 2006). Therefore, it is plausible that these east coast terrain features may cause the precipitation maximum seen in easterly wind regimes. Convergence between land breezes off the east coast and the easterly flow many also create precipitation.

3.3 DIURNAL CYCLE

3.3.1 Surface Winds

The diurnal harmonic of 3-hourly mean surface wind anomalies is plotted in Figure 3.19 (see Chapter 2.4 for methodology used). The daily land/sea breeze cycle is depicted. This variance in the wind will impact the level of convergence with incoming SW monsoon winds, which in turn may impact the generation of precipitation. Taking only these mean surface winds into account, convergence would be maximized during the night as the cool land breeze emanates outward from the island.

It is important to note that this plot only shows anomalies from the mean wind, not actual directions. For example, a vector pointed to the east at a given grid box and time does not necessarily mean that there is typically a westerly wind here. It may merely be that the mean wind at this time is *less easterly* than normal (i.e. the u-component of the wind is less negative). For example, if the fitted harmonic for the u-component of the wind in a grid box varies between 1 m s^{-1} at night and 5 m s^{-1} in the afternoon, with a daily mean of 3 m s^{-1}, this would result in a

westward-pointing vector at night (a -2 m s^{-1} anomaly, even though the wind is indeed still eastward). However, this would still impact the level of convergence. Even if the nighttime land/sea pressure gradient serves only to reduce the speed of the incoming monsoon winds (rather than reverse it into a traditional land breeze), this slowing down of the southwesterly flow could still create convergence to drive precipitation.

3.3.2 Rainfall

To get a sense of the diurnal cycle of rain, mean rain rate and rain frequency maps were calculated as in Figs. 9-10, but also divided into 3-hourly bins (Figure 3.20, Figure 3.21). Afternoon convection over the western mountains of Luzon is once again apparent during inactive periods. Any signal here of off-shore propagation of this convection is weak. Rain is very infrequent if not entirely absent over land during the overnight hours. Over the SCS, rain is scattered and infrequent in general, with a slight minimum during the afternoon. Switching to active BSISO phases, the diurnal cycle over land is once again very clear. In this case, there is a much more prominent sign of off-shore propagation, with a precipitation maximum traversing from over the mountain peaks to along the western coast between 15 and 21LT. Rainfall is relatively frequent over the ocean during all hours, with more rain in the SCS to the west of Luzon compared to the east. Offshore precipitation is the most enhanced between 03 and 06 LT, possibly due to the convergence created by the slowing down of the southwesterly flow at these times (Figure 3.19), as the monsoonal flow converges with a localized surface high pressure over the cool island at night..

A daily-mean Hovmöller diagram was also created to highlight the diurnal cycle of rain during inactive and active periods (Figure 3.22). Inactive phases demonstrate a strong diurnal cycle over the land and low mean rain rates over the ocean. Active phases show the same diurnal cycle,

but with a distinct off-shore westward propagation with time, as well as higher mean rain rates in general. The tendency for rain to fall to the west of Luzon instead of the east is also clear in the active phase plot.

3.3.3 Precipitation Features

The TRMM PF database was separated by time-of-day and BSISO phases to analyze the diurnal characteristics of raining systems during different ISO activity periods. Specifically, 30 dBZ echo heights (Figure 3.23) lightning flash rates (Figure 3.24) and PF area (Figure 3.25) were examined. The 30 dBZ echo heights and lightning flash rates provide a measure of the intensity of the storms and strength of the convective updrafts (Petersen et al. 1996; Zipser and Lutz 1994), while PF sizes can give a sense of the organization and mode of precipitation systems (i.e. large MCS's versus small isolated convective cells).

During inactive BSISO phases, deep convection with relatively high flash rates is common in the afternoon (15-18 local time) over land. Aided by the reduced cloud cover during inactive periods (Figure 3.7), strong solar insolation generates more instability which promotes these strong storms. Looking at the size of the PFs over land, there is some evidence of upscale growth of these afternoon storms. At 15 local time (LT), many small PFs (<2000 km^2) are evident over the northern mountain peaks. By 18 LT the number of PFs in this area is reduced, but there are more large PFs (>10000 km^2), and they appear to have shifted slightly to the SW. This may be indicative of smaller isolated cells forming over the highest terrain, and then moving westward and merging into larger storm complexes. Over the SCS to the west, convection is typically weaker (lower 30 dBZ heights, reduced lightning) than over land. The strongest over-ocean PFs are found to the west of Luzon during the overnight/early morning hours (00-06 LT).

During active BSISO phases, enhanced cloud shading is expected to hamper the instability generated over land, thereby reducing the likelihood of afternoon convection. However, a diurnal cycle is still noted over land even during active phases, albeit with slightly weaker storms (lower 30 dBZ echo heights and flash rates) compared to inactive periods. As mentioned previously, the diurnal cycle of land precipitation has been found to be instrumental to generating the off-shore convection seen in other regions. So, it is important to note that a diurnal cycle still exits over Luzon even during the active BSISO. Over the SCS, PFs with moderate 30 dBZ heights and some lightning were more widespread in active conditions compared to inactive. Large raining systems (>40000 km^2) were also much more frequent. This is likely the result of large organized monsoon rain bands and MCSs traversing across the region during these active monsoon periods.

3.4 VERTICAL STRUCTURE

While rainfall information is useful to determine the location of precipitation, not much can be gleaned in terms of the structure of the convection from these data alone. Towards this goal, the vertical structure of precipitating systems was analyzed using reflectivity profiles from TRMM PR and GPM KuPR across different BSISO phases and the diurnal cycle. Figure 3.26 consists of histograms of echo top heights along a longitudinal band across the study region during inactive and active phases, respectively. Here, echo top heights are defined as the highest vertical point that the radar detected its minimum reflectivity (~17 dBZ for PR and KuPR). Because data is gathered across a longitudinal band, it is desirable for the coast line in this band to run approximately North-South, to avoid mixing radar data from the land and sea. For this reason, only reflectivity profiles within 16-18° N were compiled in this analysis. This also corresponds with where the tallest mountain peaks are located.

In general, the tallest echoes occur most frequently over high terrain. Evidently the orographic enhancement along with strong daytime instability produce the updrafts needed for deep convective cores. Very tall afternoon storms are more frequent in inactive phases than active phases over the mountains (57% more storm tops over 10km from 12-20 LT, 120-122 °E) corresponding with the greater instability shown previously. There also appears to be a delay in the onset of deep convection in active BSISO phases, possibly due to cloud shading increasing the time needed triggering surface-based convection. Westward off-shore propagation of this convection is once again apparent during active phases. Higher echo tops become less frequent as this convection moves further into the SCS, suggesting possible upscale growth into more stratiform-dominated systems. A nocturnal maximum in oceanic precipitation is noted in active phases, contrasting with the afternoon peak over the land.

Median vertical profiles of reflectivity over land and ocean during inactive and active BSISO phases are shown in Figure 3.27. Additionally, profiles of reflectivity anomalies were produced by taking the difference between each profile and a mean of the four profiles (Figure 3.28). The deepest and strongest convection is once again noted over the land during inactive phases. Anomalously high reflectivity is seen at the lower and upper levels. A strong melting layer signature is present around the freezing level (5km) in the oceanic active BSISO profile. During active periods, large, organized convective systems move over the ocean with well-developed stratiform regions. Part of this may be from land-based convection growing upscale and propagating as a mature MCS into the SCS. Conversely, the over-land inactive reflectivity anomaly profile in Figure 3.28 has lower values around the freezing level, indicating that convection is more predominant than stratiform precipitation.

Individual DPR KuPR overpasses are examined in Figure 3.29. During inactive days, isolated convection initiates over the mountains (Figure 3.29a). These storms may eventually develop into an organized squall line which propagates off-shore (Figure 3.29c). In this case, off-shore propagation occurred early in the afternoon, as opposed to the typical nocturnal off shore propagation. In each case, cross-sections show the strongest convection over elevated terrain (Figure 3.29b, 3.29d). Although the signal for these off-shore propagating convective systems during inactive phases was not seen in the mean rainfall plots described previously, it is still thought to occur at least occasionally. During active phases, oceanic precipitation is widespread and frequent. Organized convective systems move off the coast in the afternoon (Figure 3.29e), and moderate stratiform rainfall persists overnight (Figure 3.29g) with defined melting layer signatures (Figure 3.29h). It is important to note that these are individual snapshots of precipitation from different days. Although concepts like off-shore propagation are theorized to occur, the satellite radars do not provide the temporal resolution needed to capture this happening on a single-case basis.

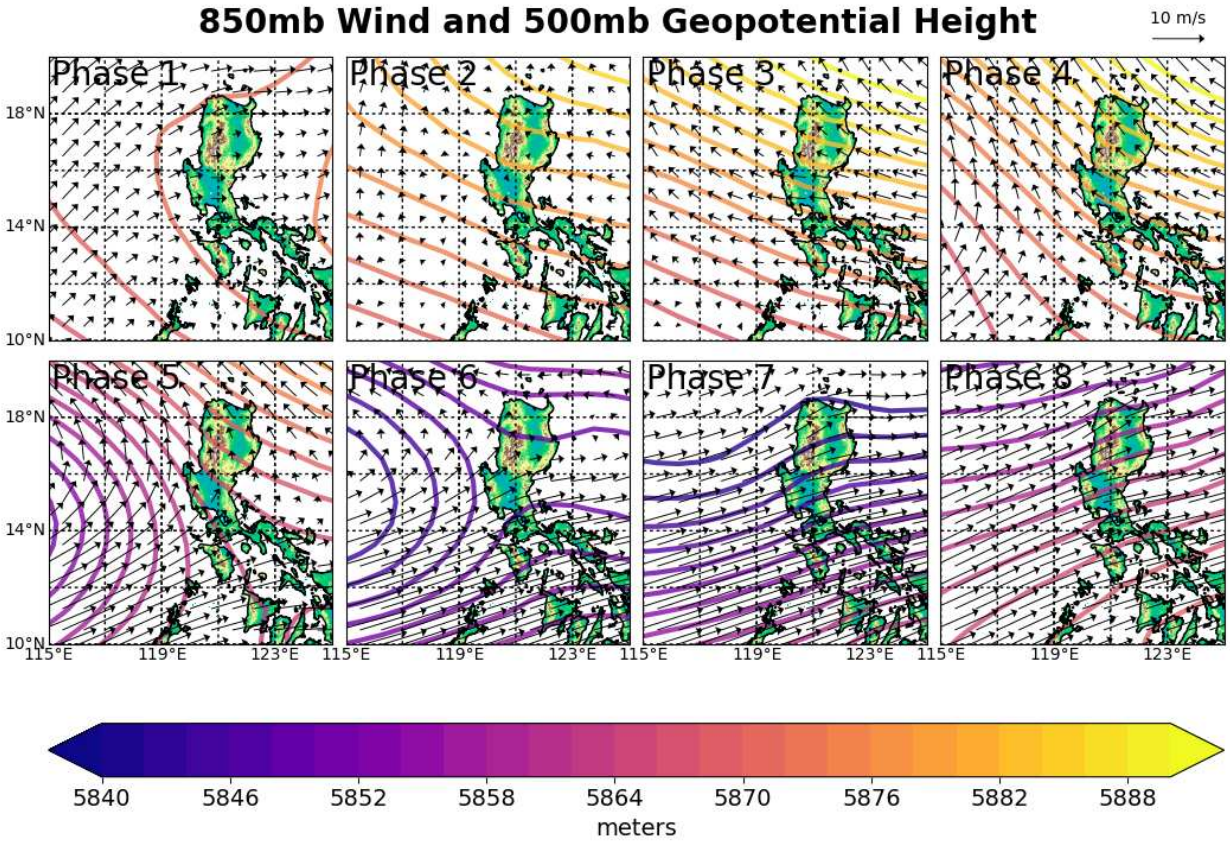

Figure 3.1: Mean 850mb winds (vectors) and 500mb geopotential heights (contours) from ERA-Interim Reanalysis across different BSISO phases.

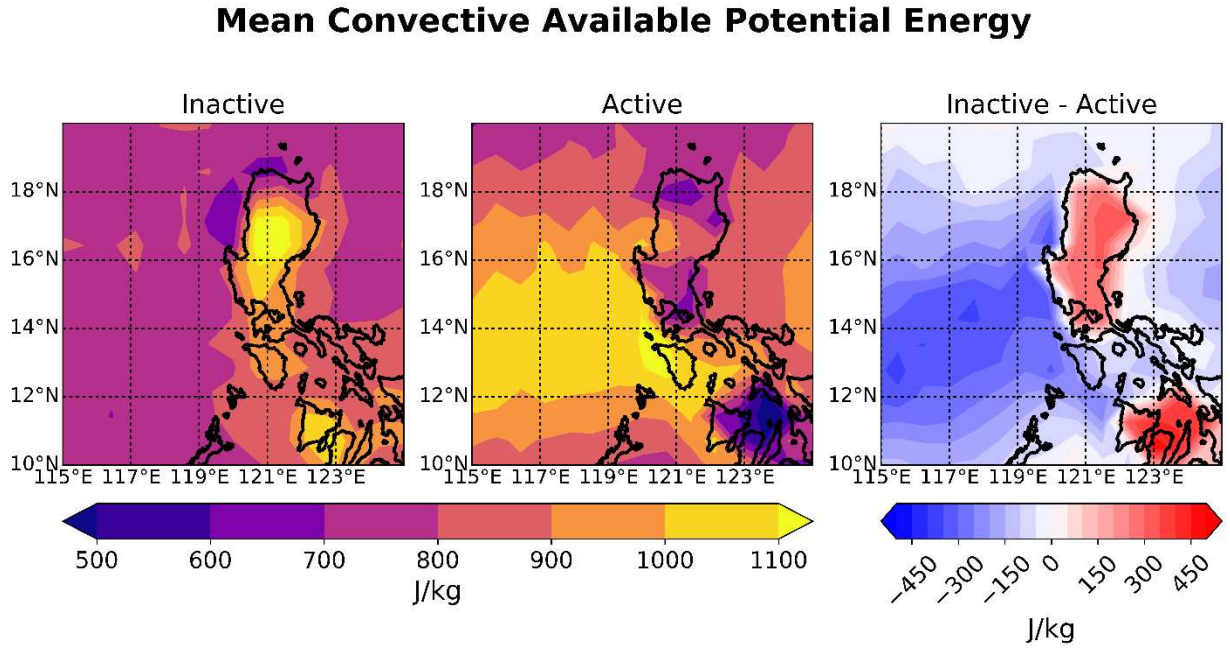

Figure 3.2: Mean convective available potential energy from ERA-Interim Reanalysis during inactive and active BSISO phases.

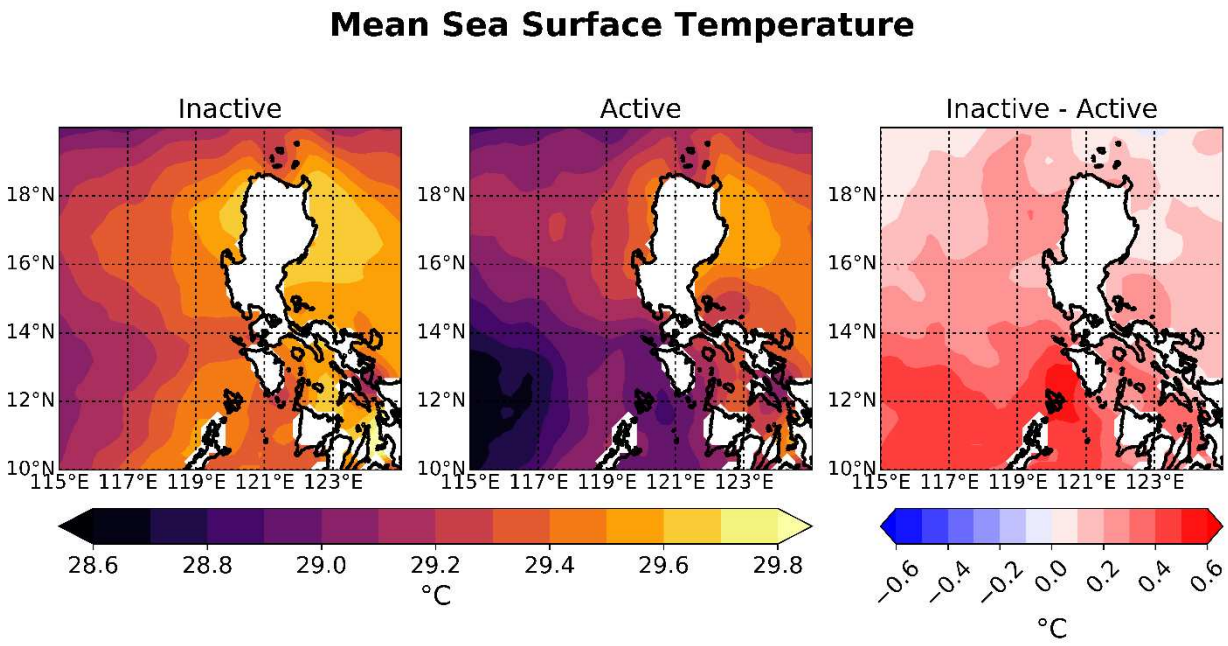

Figure 3.3: Mean sea surface temperatures from NOAA OI during inactive and active BSISO phases.

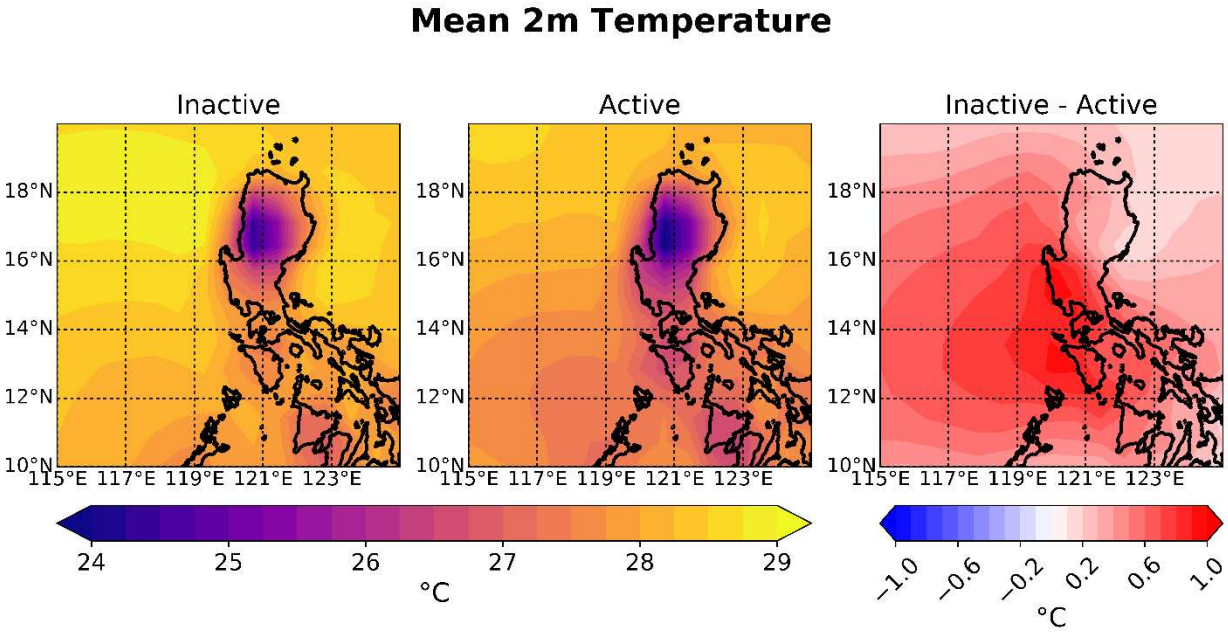

Figure 3.4: Same as Figure 3.2, but for 2m air temperature

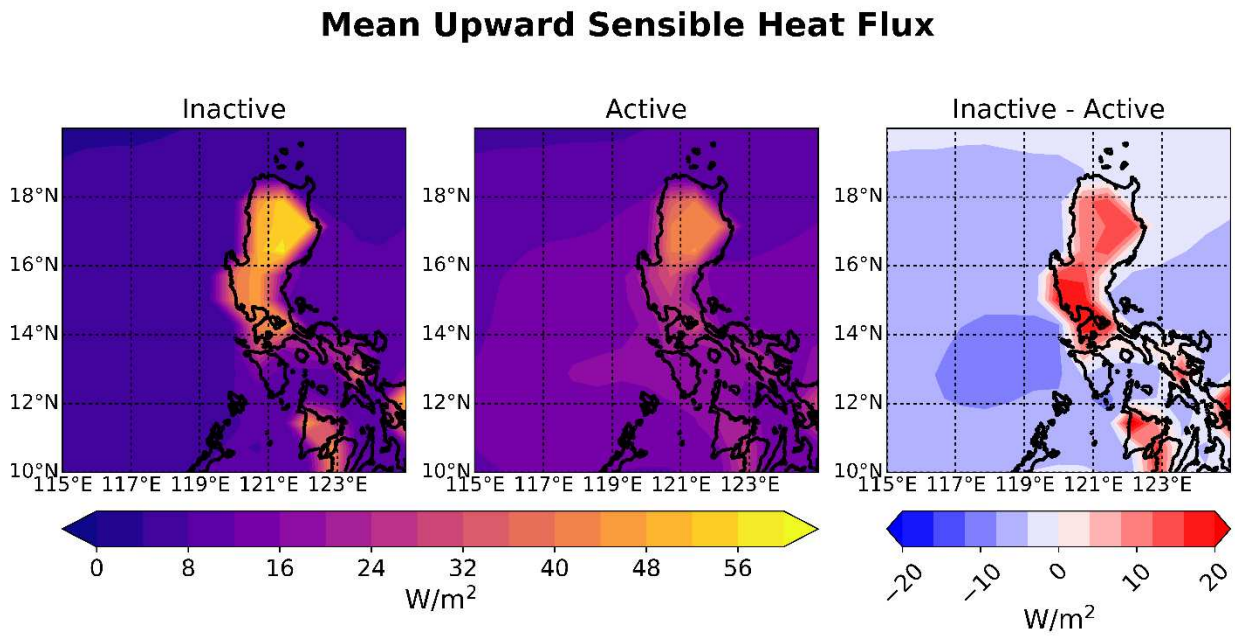

Figure 3.5: Same as Figure 3.2, but for sensible heat flux. Positive values in the left and center image denote upward fluxes.

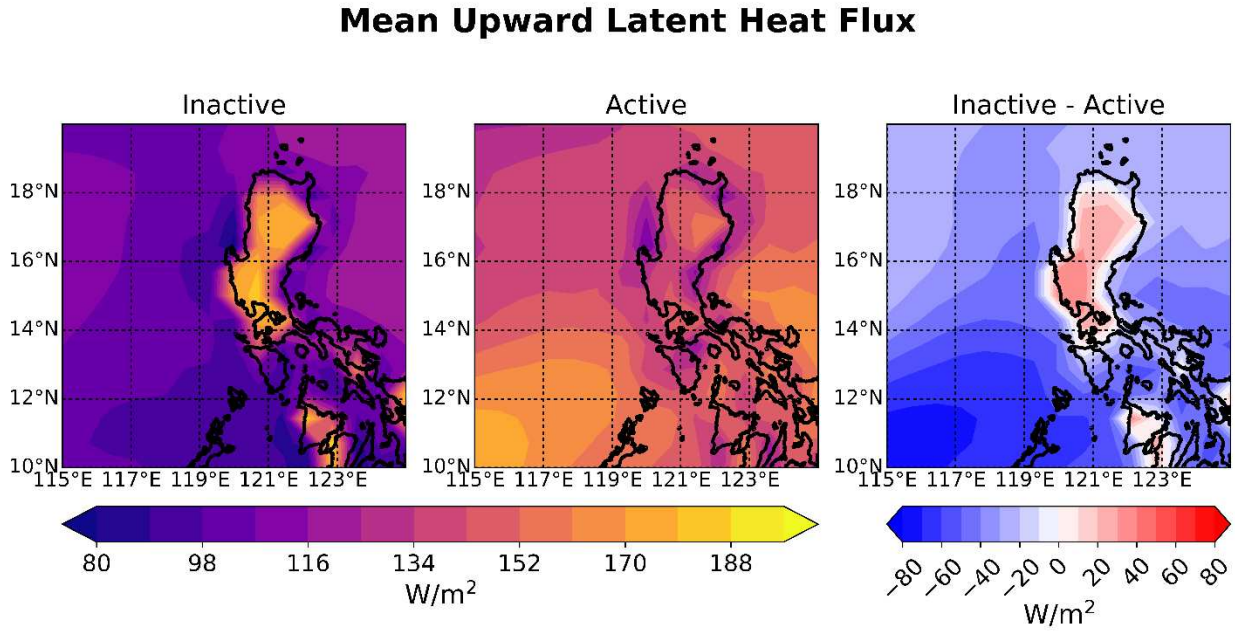

Figure 3.6: Same as Figure 3.5, but for latent heat flux.

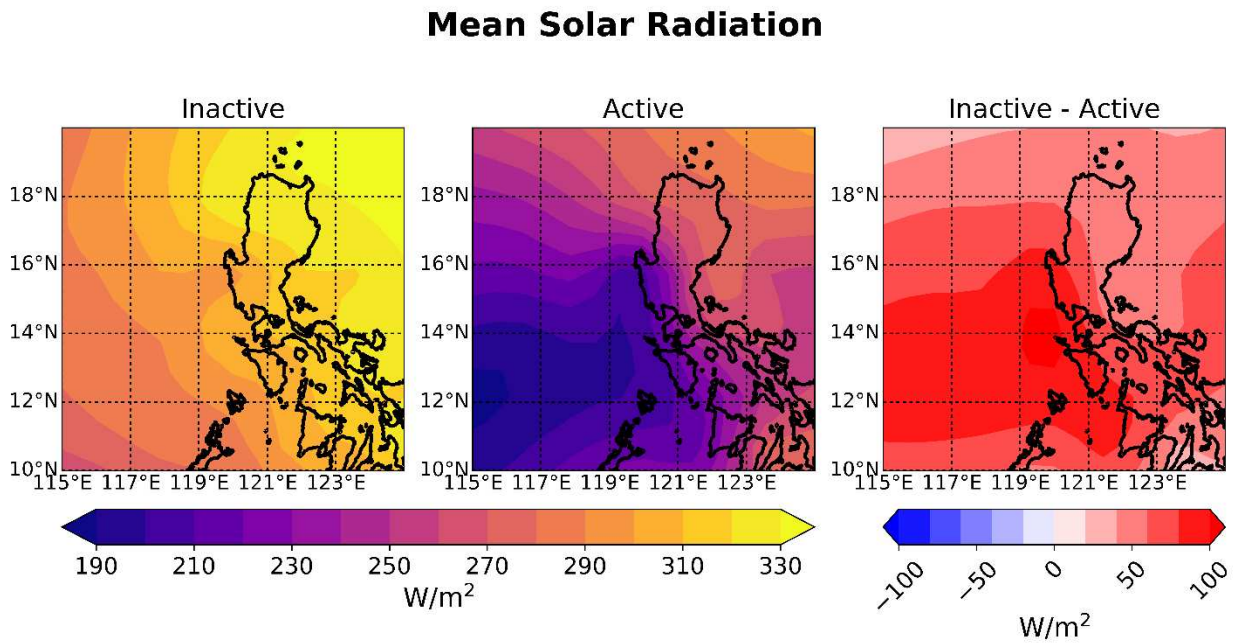

Figure 3.7: Same as Figure 3.2, but for downwelling solar radiation.

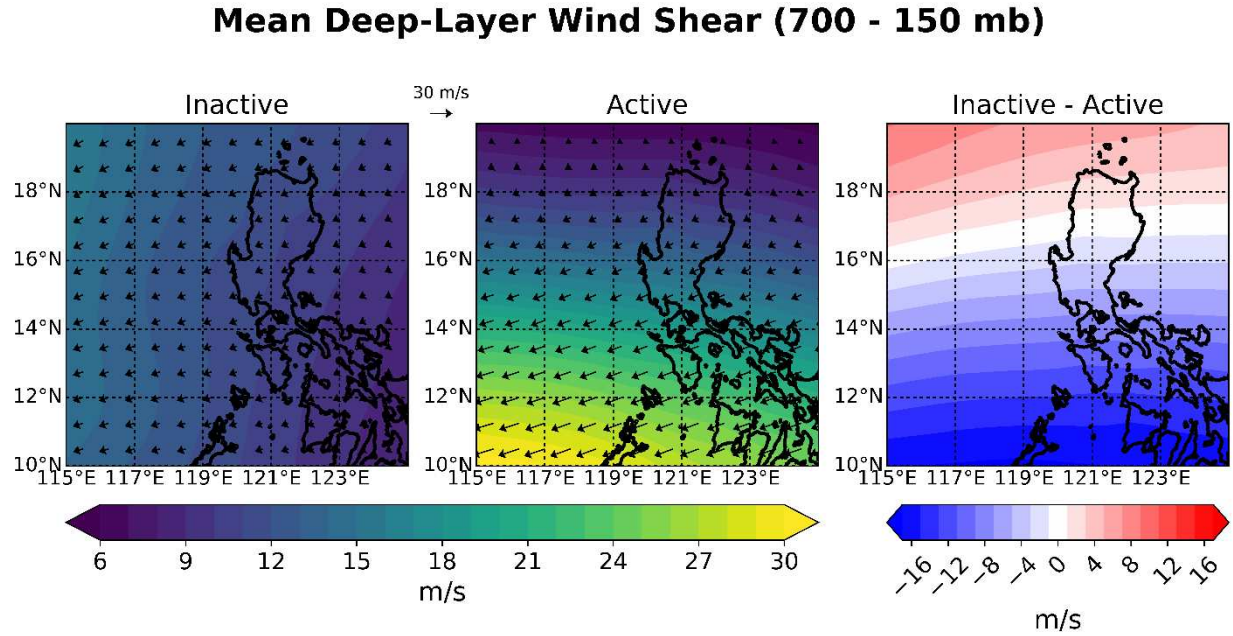

Figure 3.8: Mean 700-150mb wind shear from ERA-Interim Reanalysis during inactive and active BSISO phases. Vector differences are also plotted.

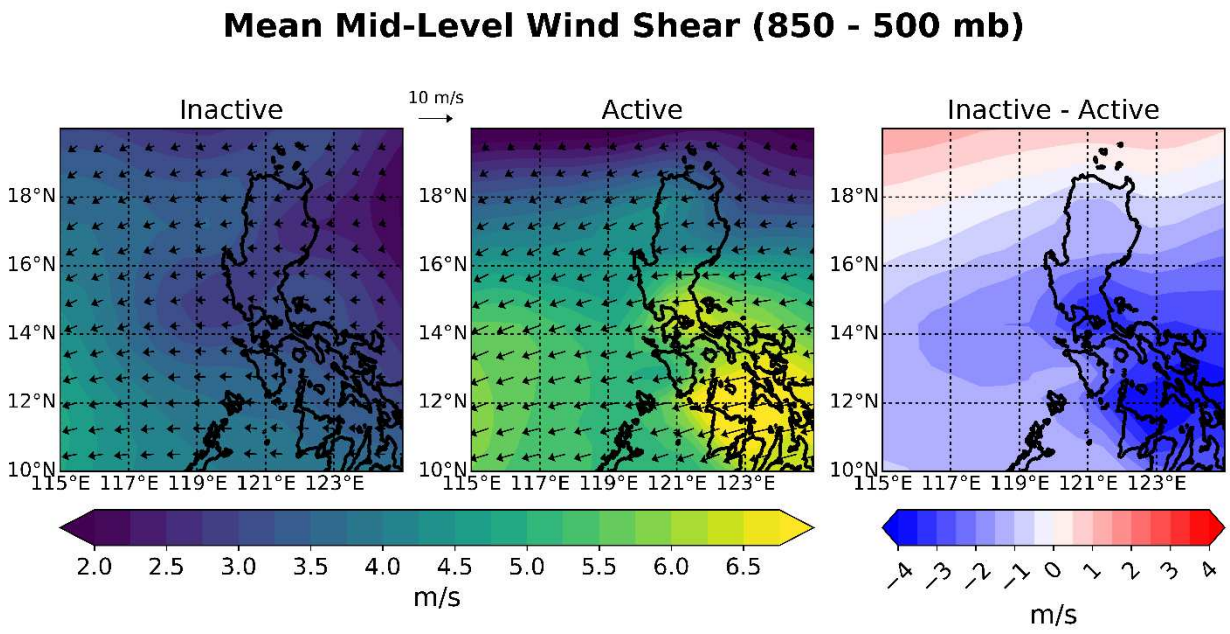

Figure 3.9: Same as Figure 3.8, but for 850-500mb wind shear

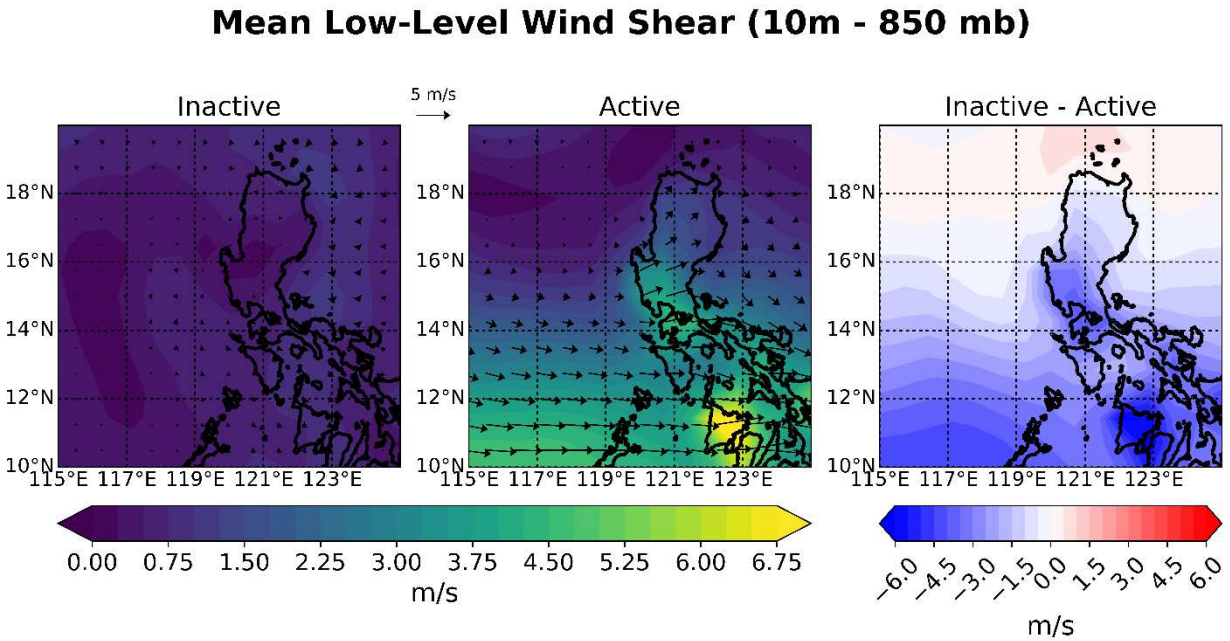

Figure 3.10: Same as Figure 3.8, but for 10m – 850mb wind shear.

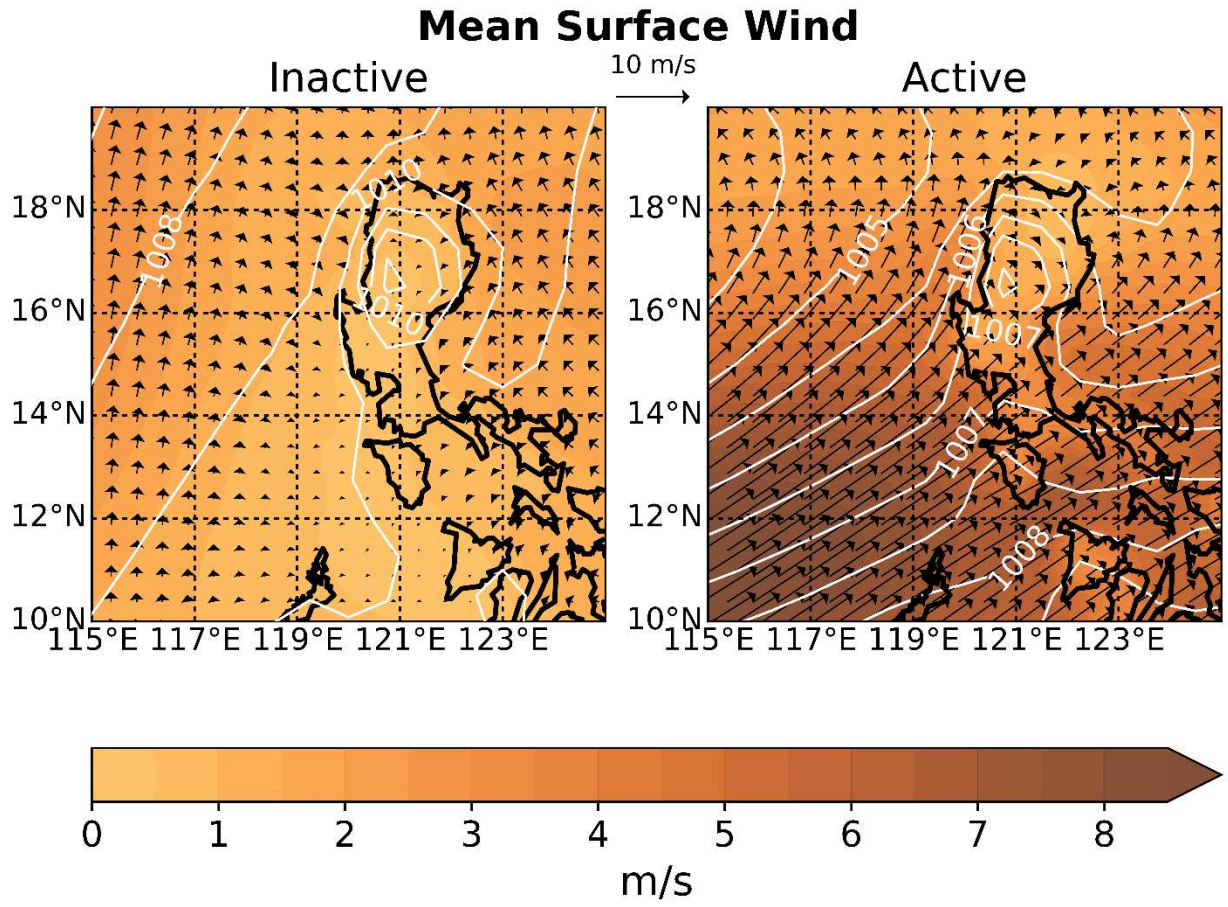

Figure 3.11: Mean wind vectors and speed (shading) from CCMP, and ERA-Interim mean sea level pressure (contours) during inactive and active BSISO phases

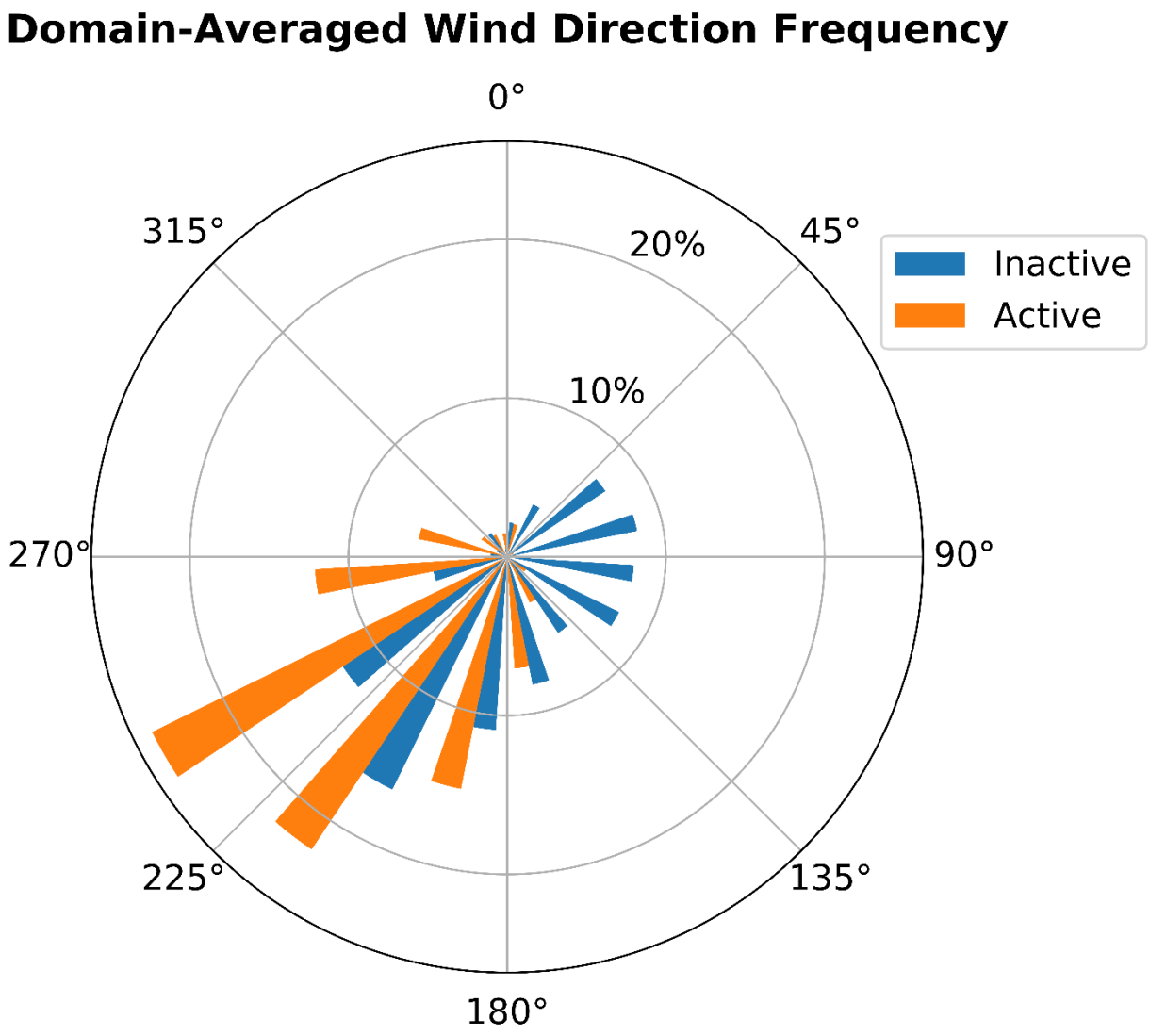

Figure 3.12: Frequency of domain-averaged wind direction from CCMP during TRMM/DPR overpasses for inactive and active BSISO phases

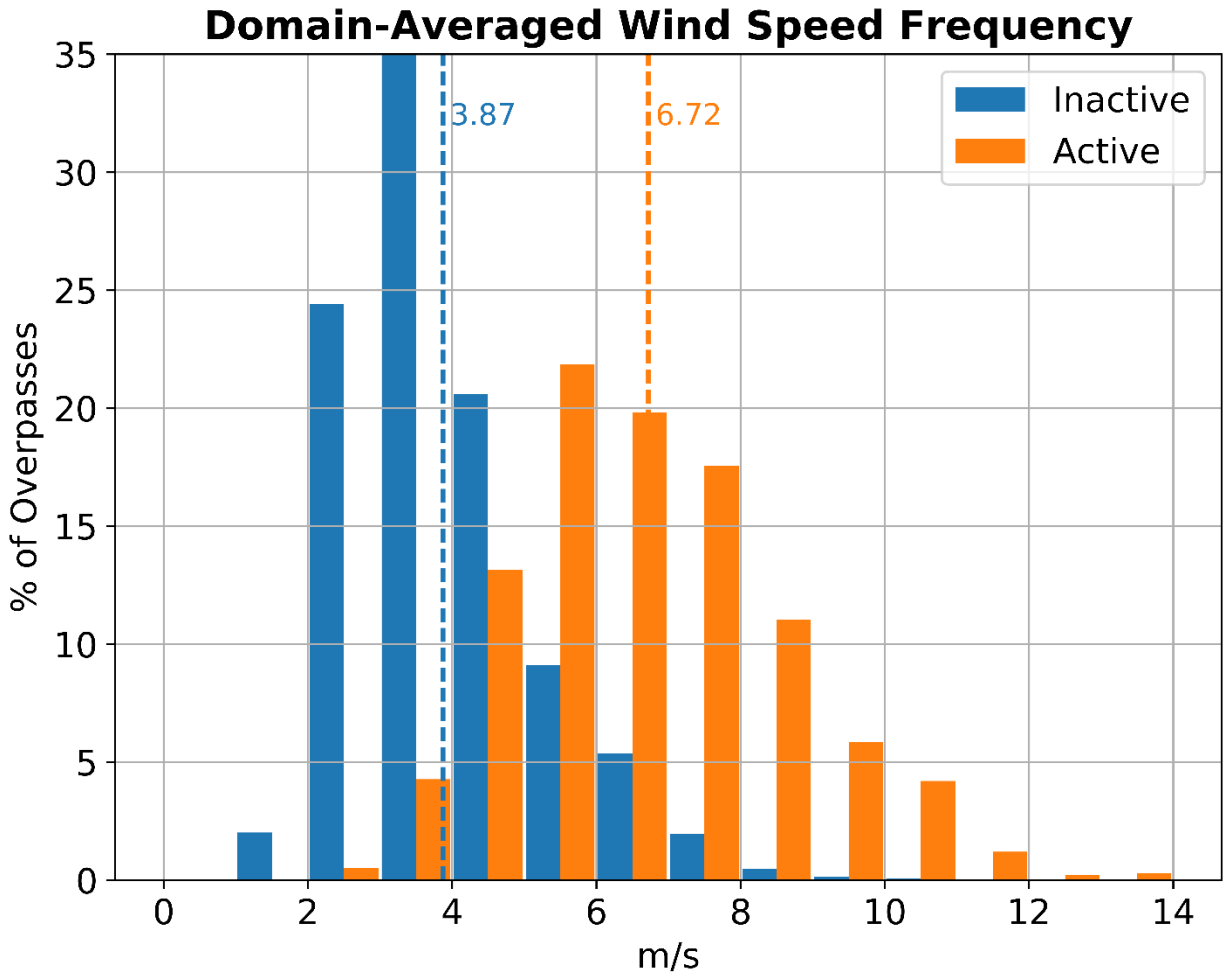

Figure 3.13: Same as Figure 3.12, but for wind speed. Dotted lines indicate the mean of the distribution of the same color.

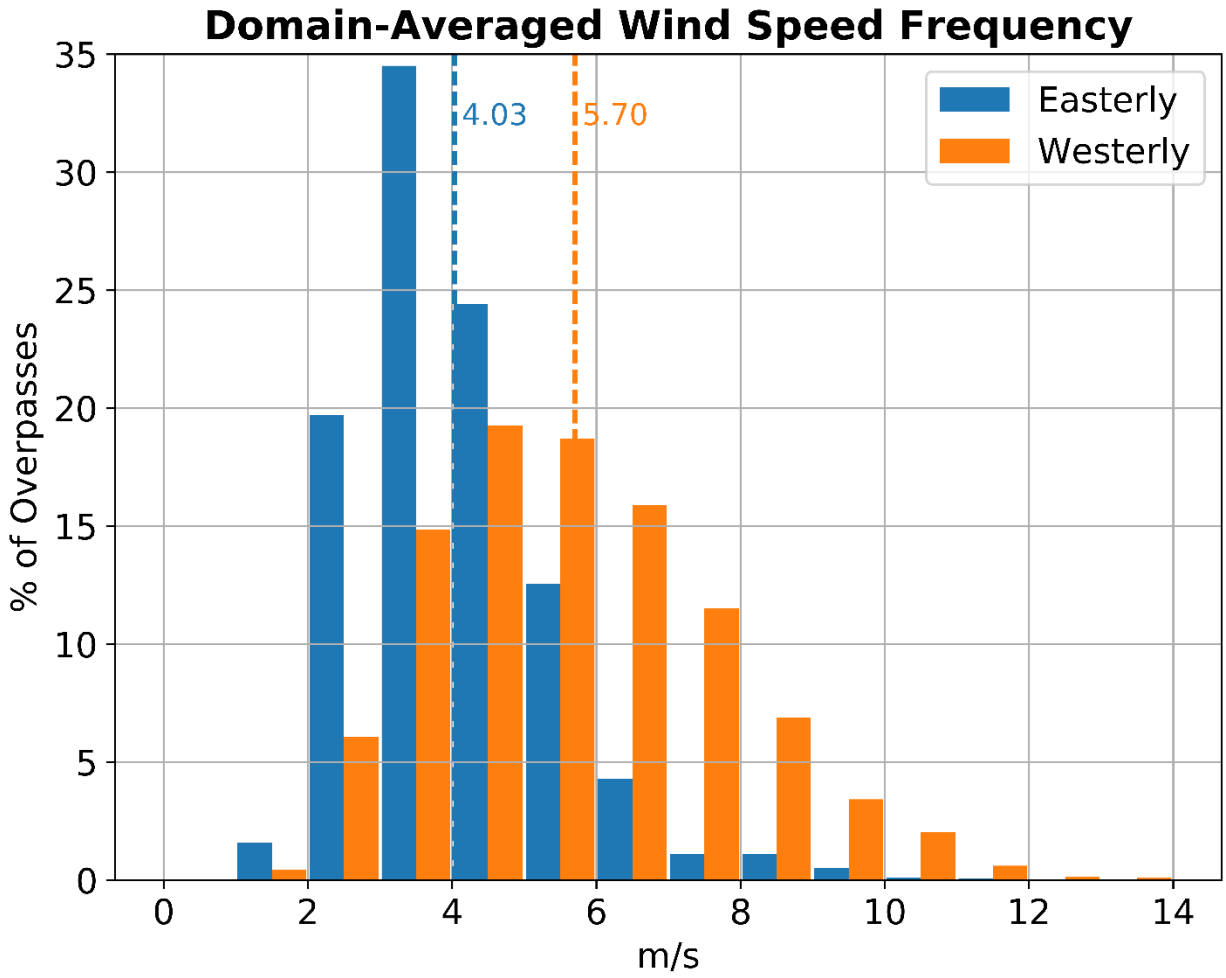

Figure 3.14: Same as Figure 3.13, but separated by domain-mean wind direction rather than BSISO phase.

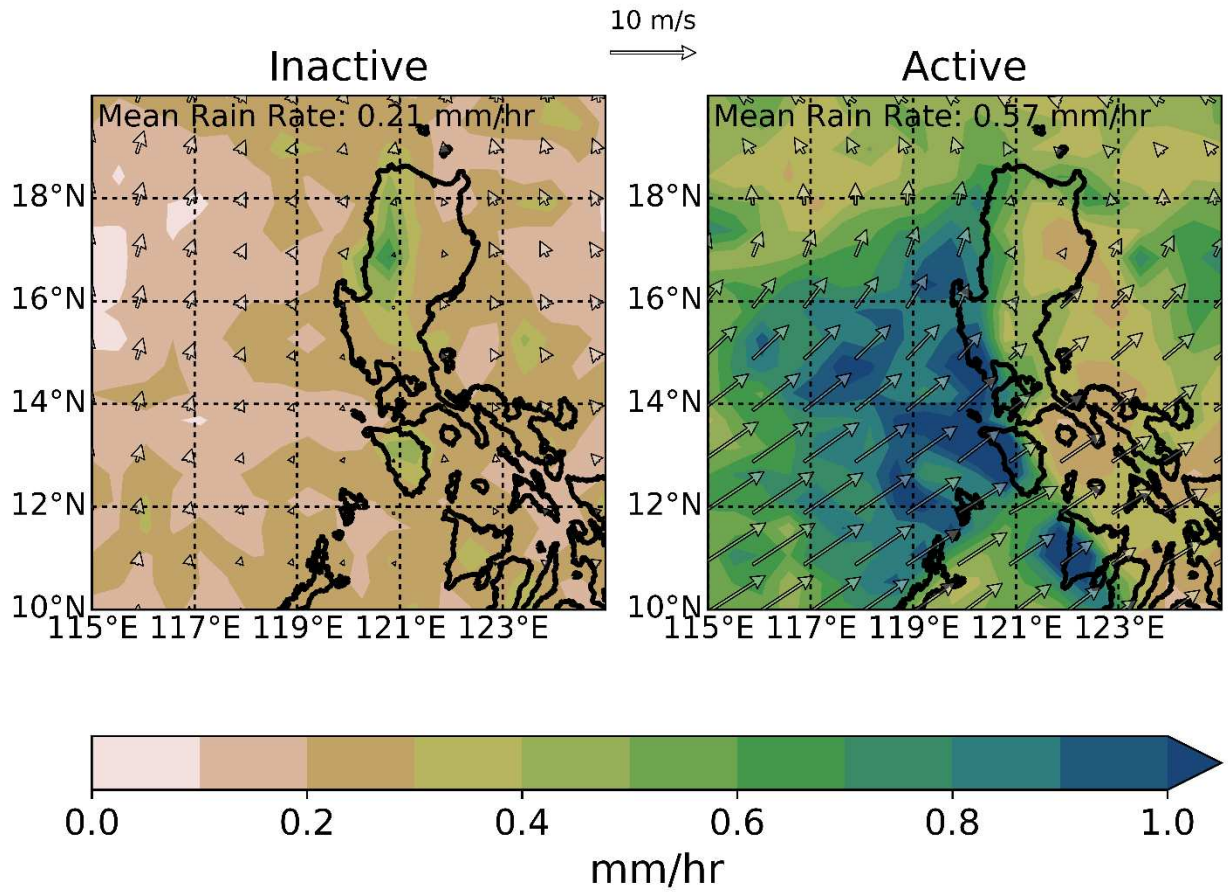

Figure 3.15: Mean rain rate measured by TRMM PR and DPR KuPR during inactive and active BSISO phases. Overlaid with mean wind vectors from CCMP, as in Figure 3.11. The mean rain rate across the domain is written in the upper portion of each subset figure.

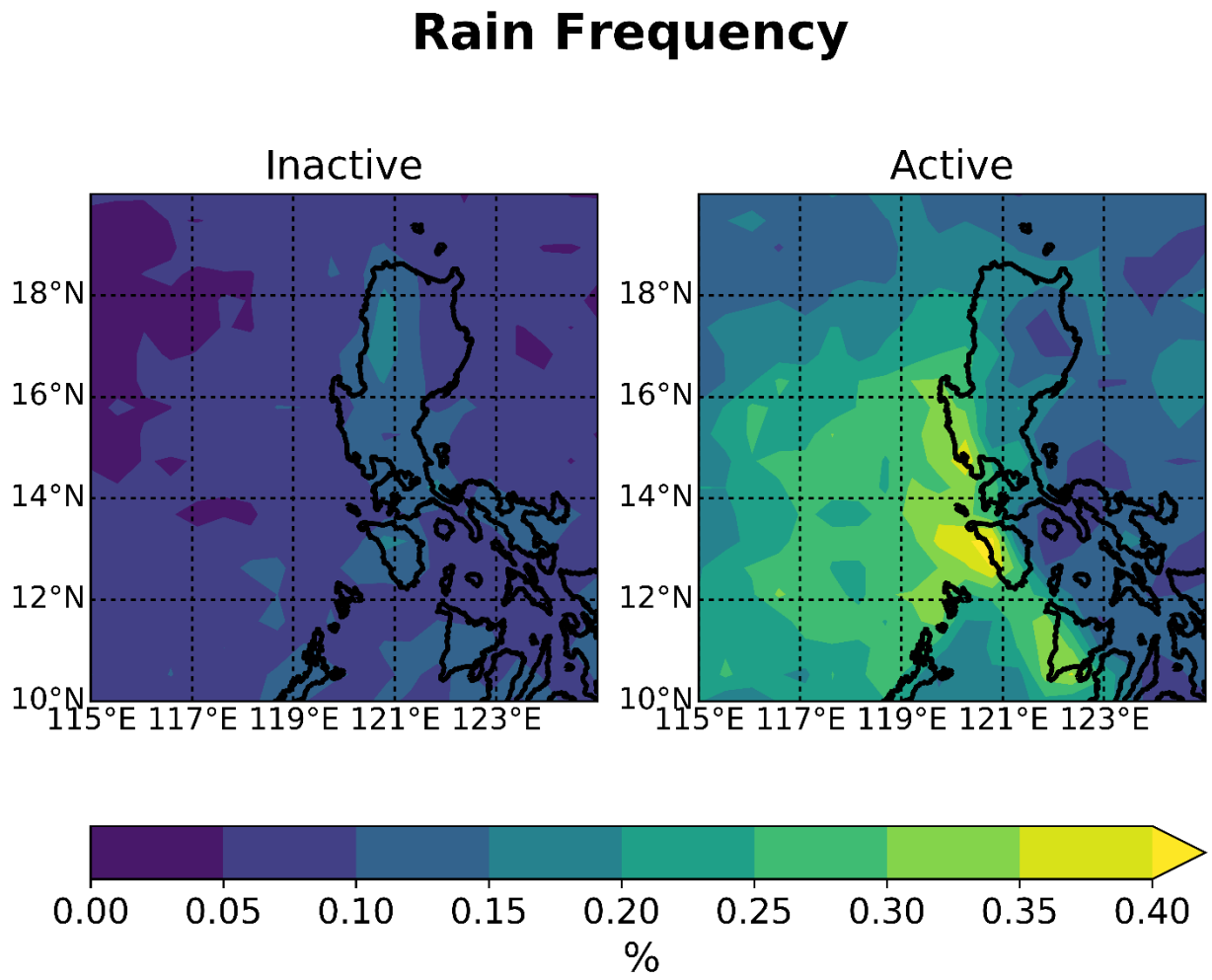

Figure 3.16: Percent of TRMM/DPR overpasses which saw rain in the area for inactive and active BSISO phases.

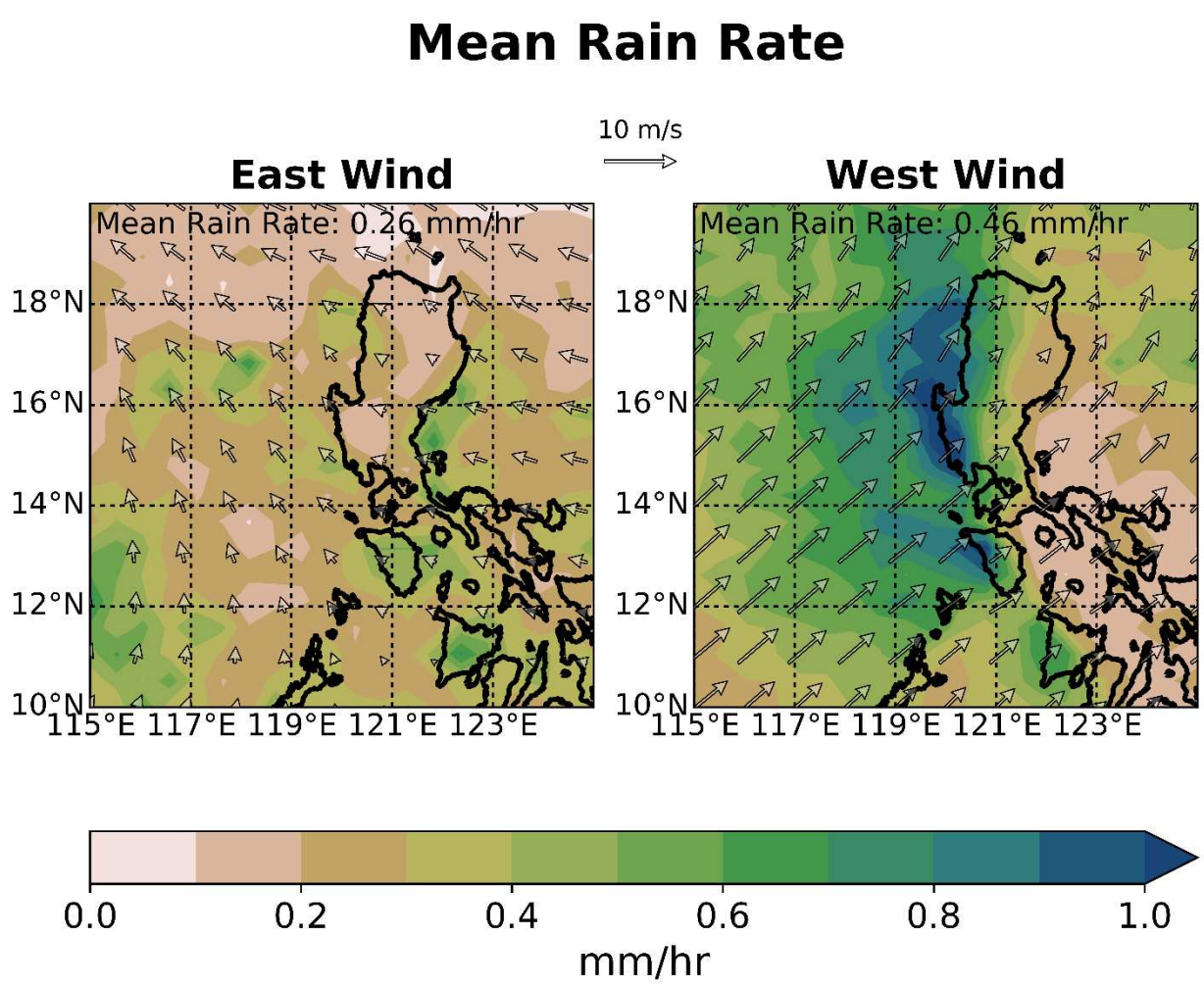

Figure 3.17: Same as Figure 3.15, but separated by domain-mean wind direction rather than BSISO phase.

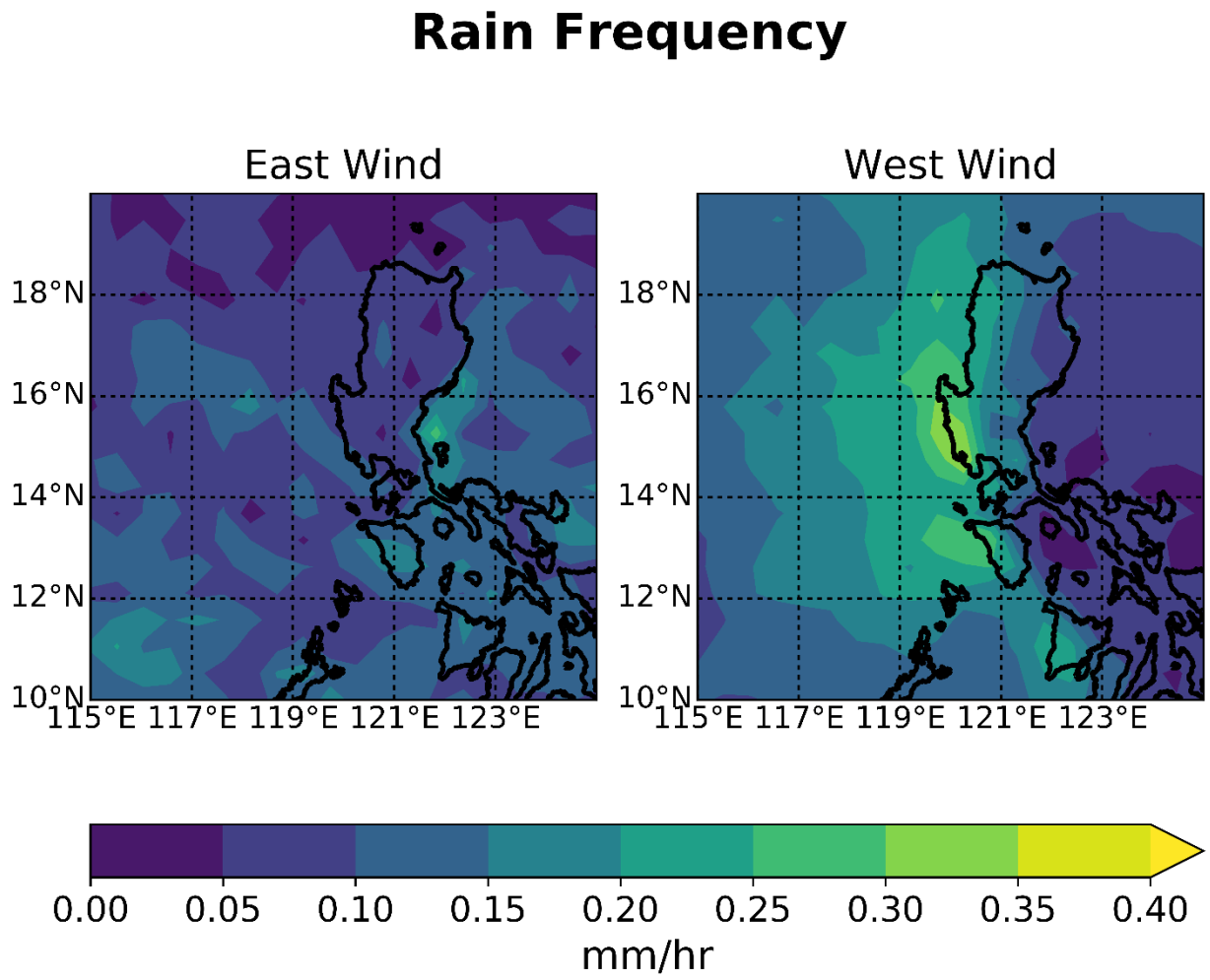

Figure 3.18: Same as Figure 3.17, but for rain frequency.

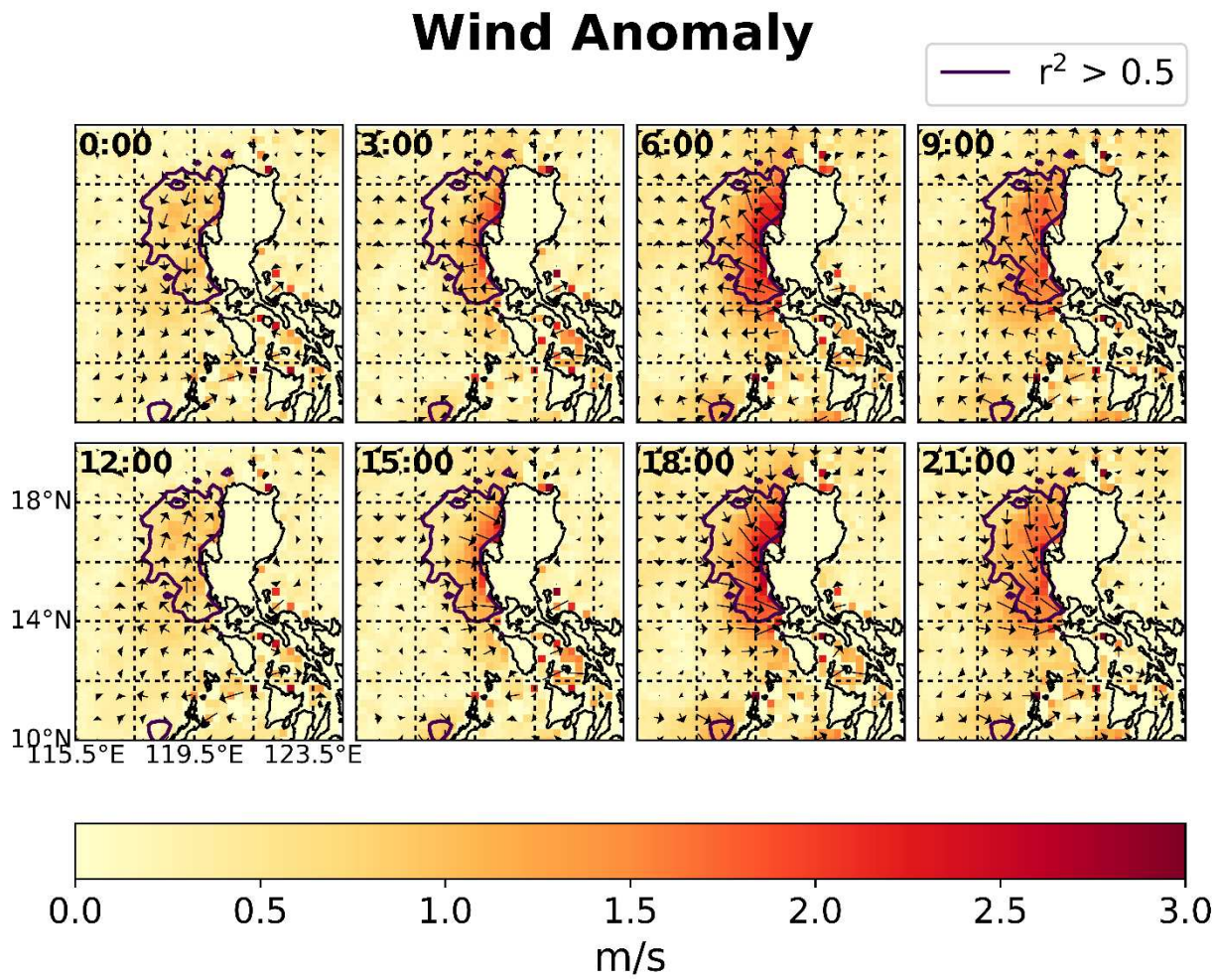

Figure 3.19: Diurnal harmonic wind anomaly vectors and magnitude (shading) based on surface wind measurements by the RapidScat scatterometer. Areas inside the blue contour are fitted to the diurnal harmonic with an r^2 value of > 0.5. Timestamps are in local time (UTC + 8).

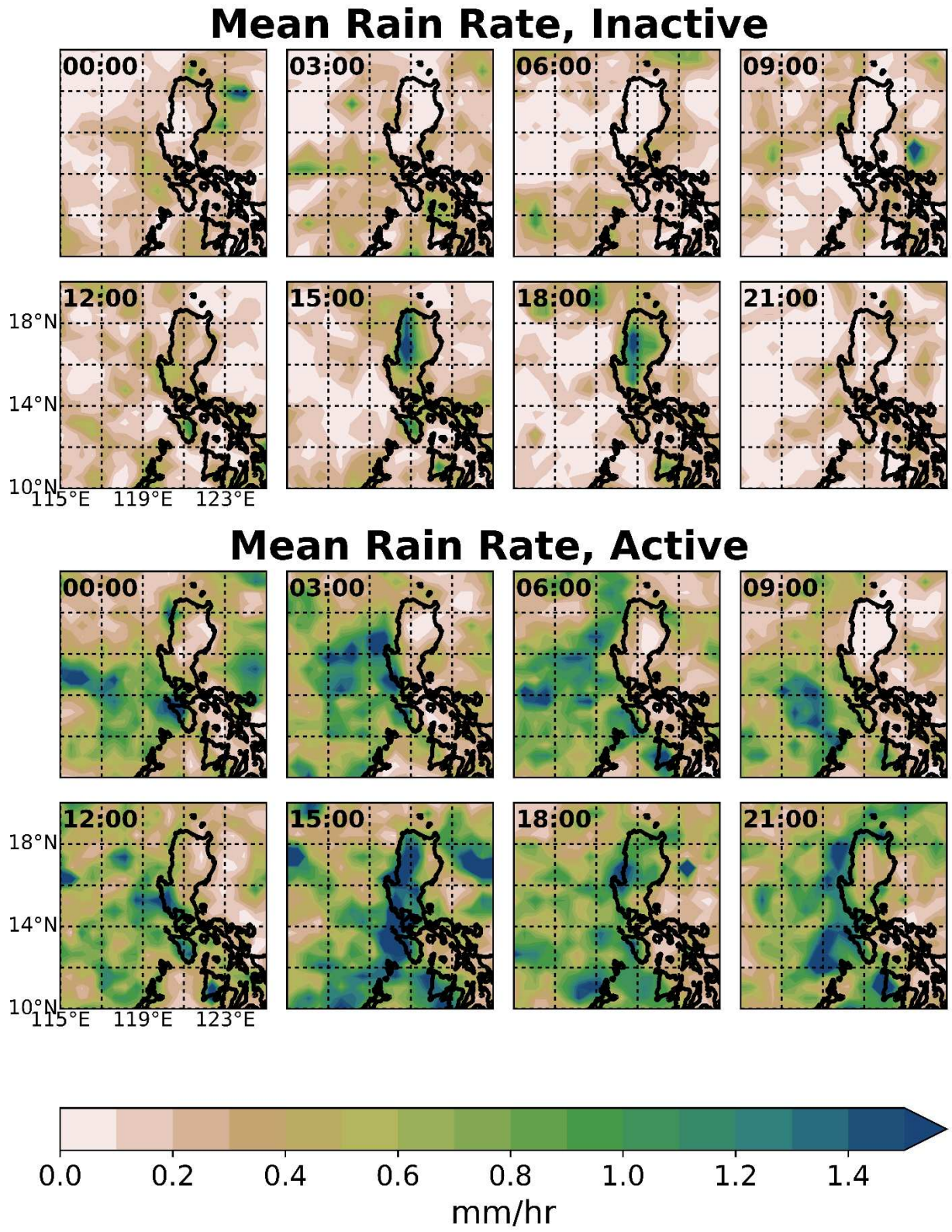

Figure 3.20: Same as Figure 3.15, but subdivided further into 3-hourly bins. Timestamps are in local time (UTC + 8). Time bins are centered on the timestamp in the upper-left of each figure

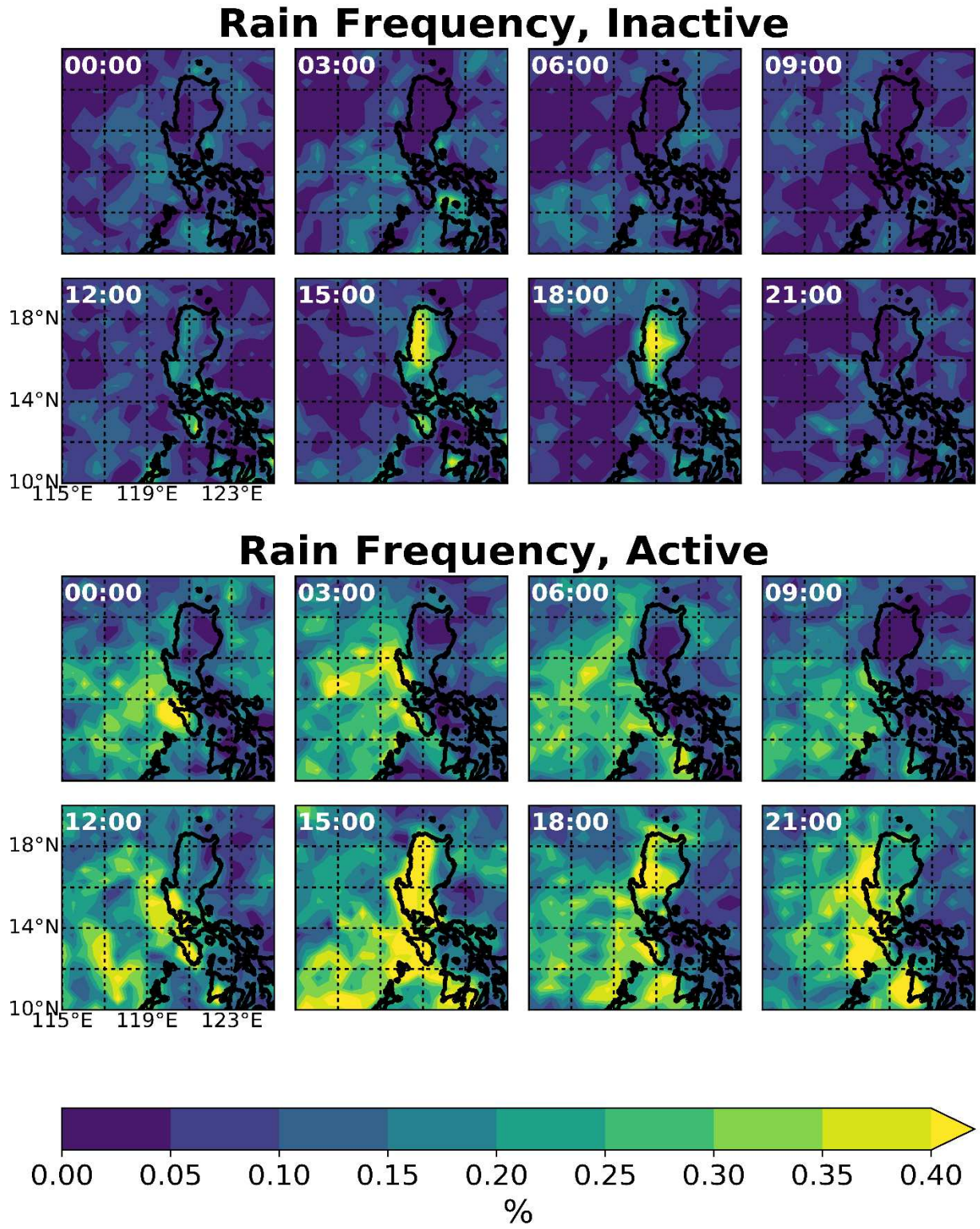

Figure 3.21: Same as Figure 3.20, but for rain frequency.

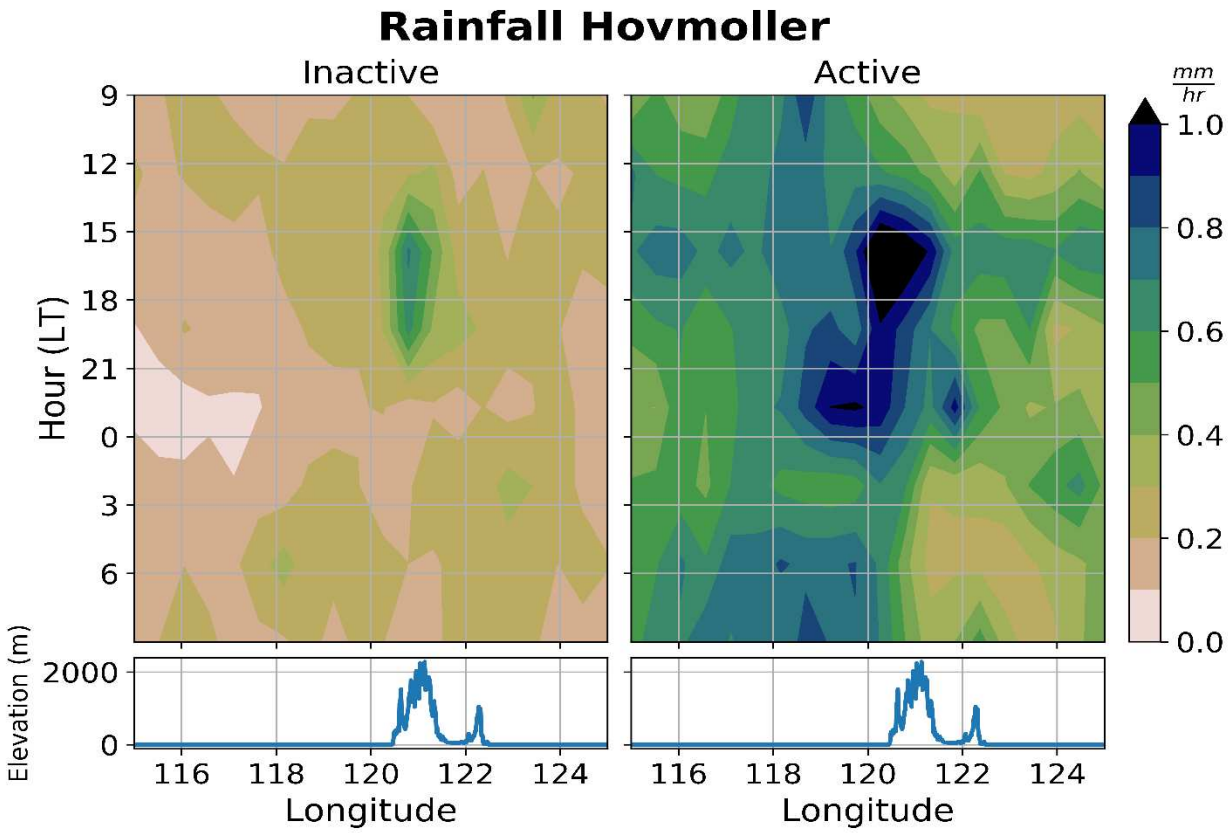

Figure 3.22: Mean daily Hovmöller diagram of rain rate during inactive and inactive periods of the BSISO. Bottom plots show the land topography along 17 °N

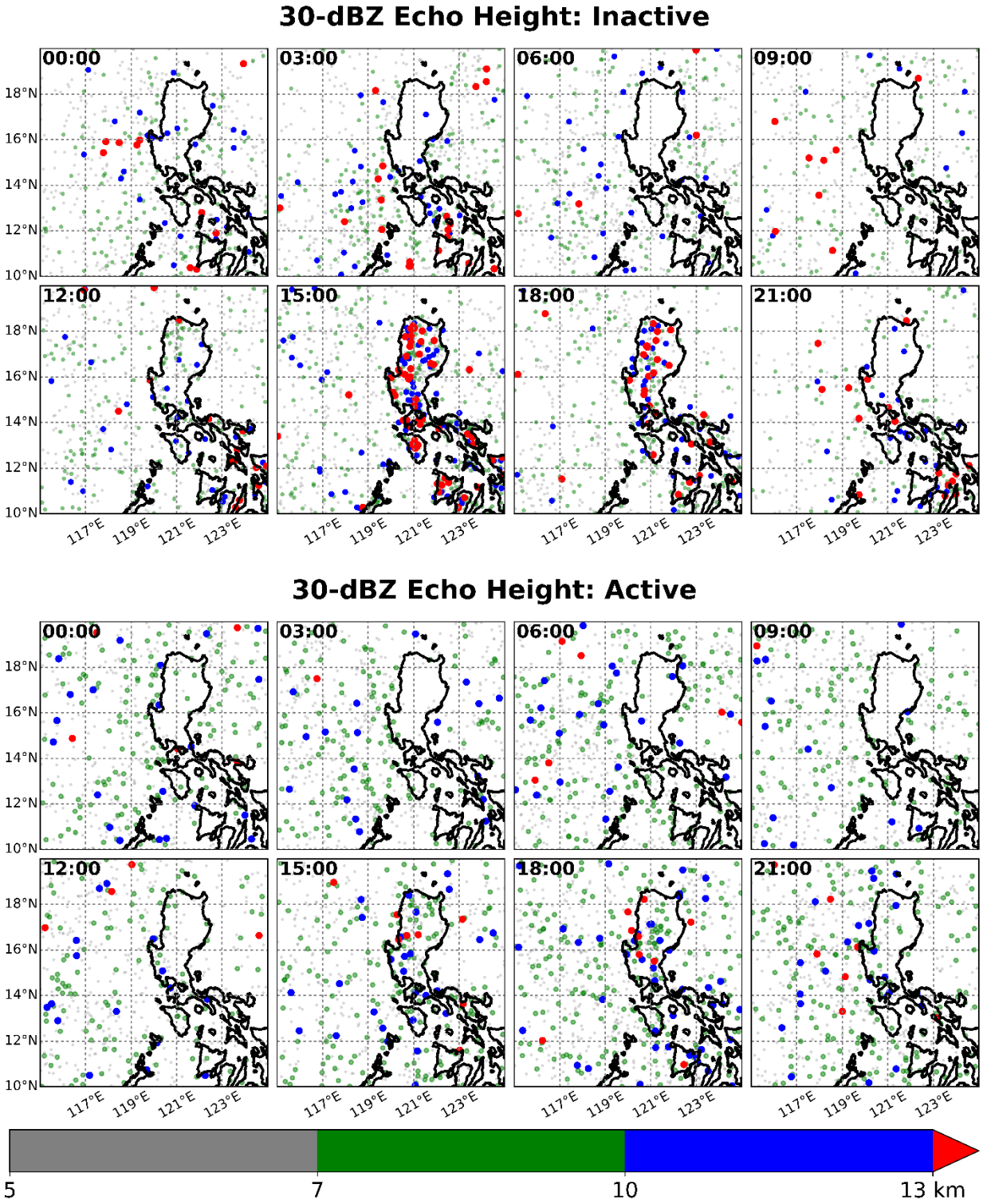

Figure 3.23: Scatter plot of 30 dBZ echo heights of TRMM precipitation features during inactive and active BSISO phases. Timestamps are in local time (UTC + 8)

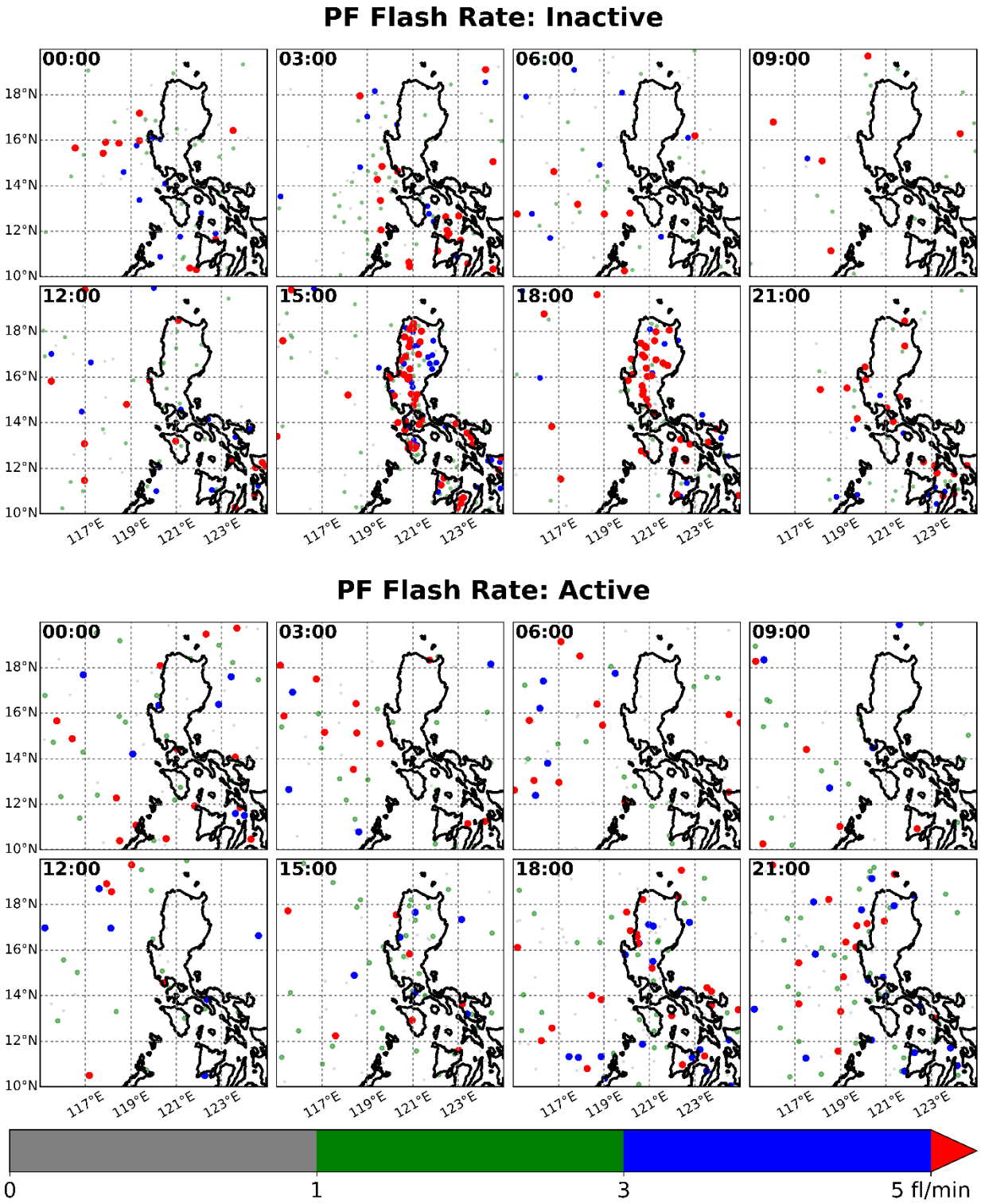

Figure 3.24: Same as Figure 3.23, but with precipitation feature flash rate.

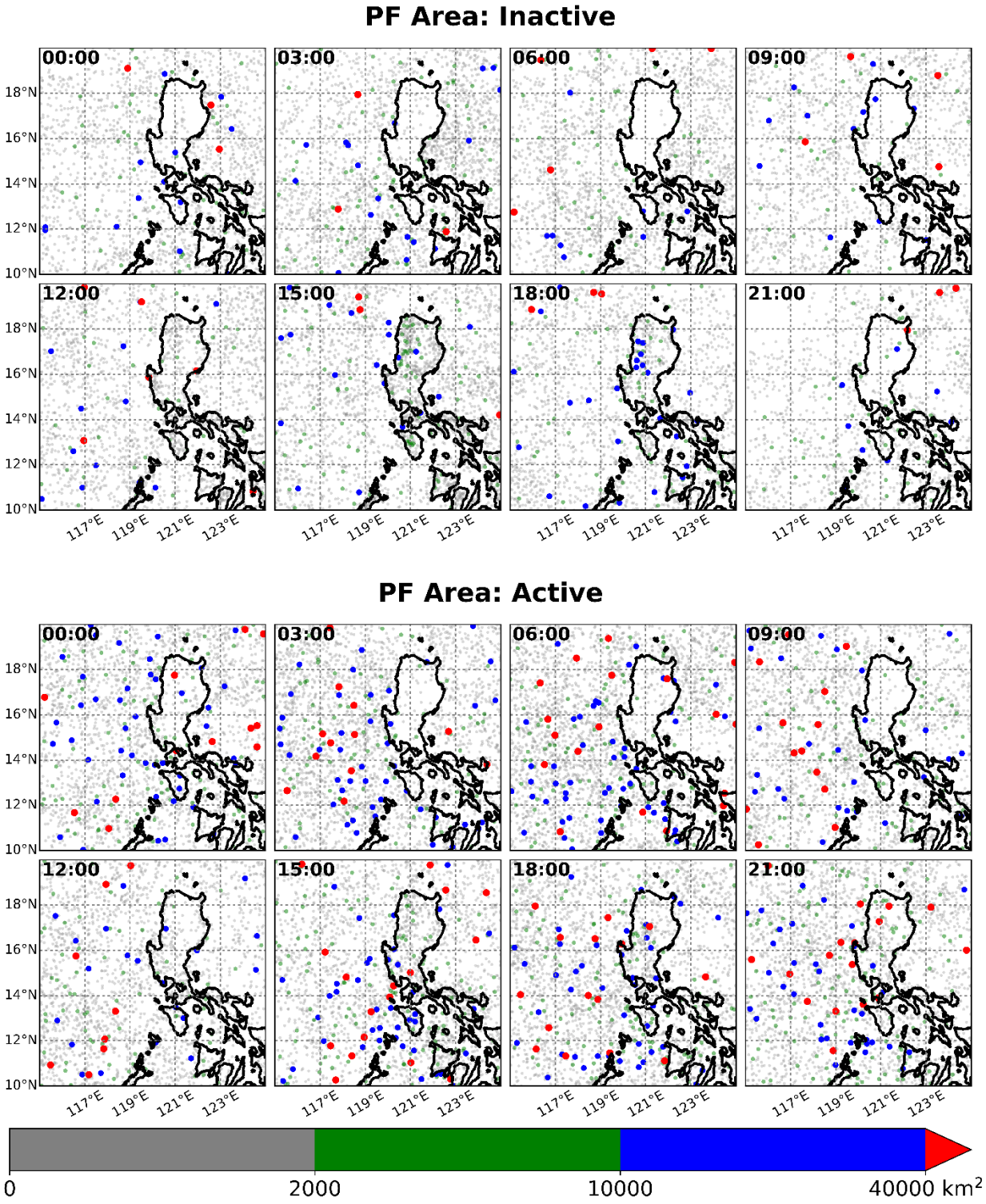

Figure 3.25: Same as Figure 3.23, but with precipitation feature area.

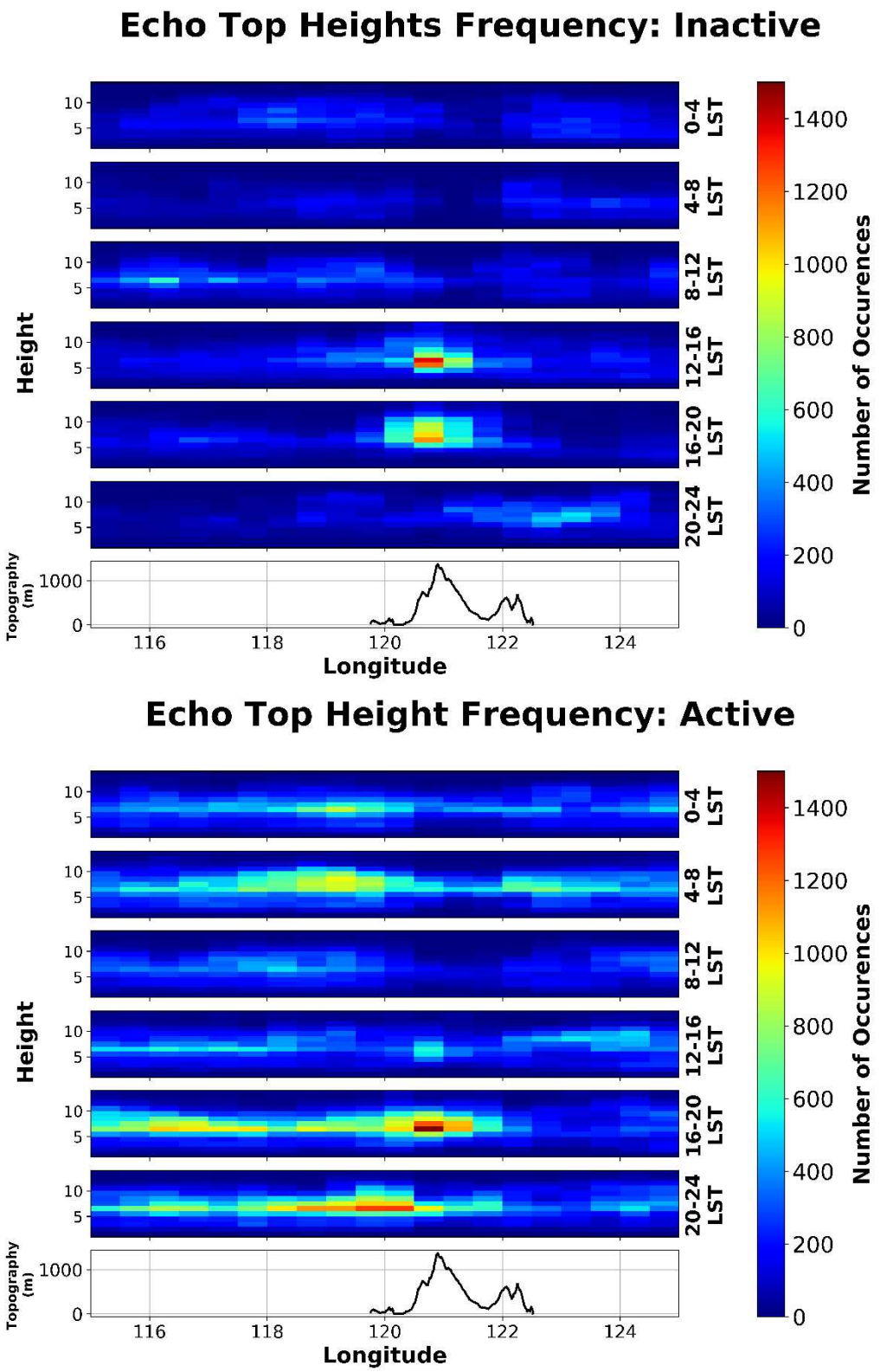

Figure 3.26: 2-D histograms of echo-top heights measured by TRMM PR and DPR KPR as a function of time-of-day, during inactive and active BSISO periods. Terrain height is given in the bottom plot.

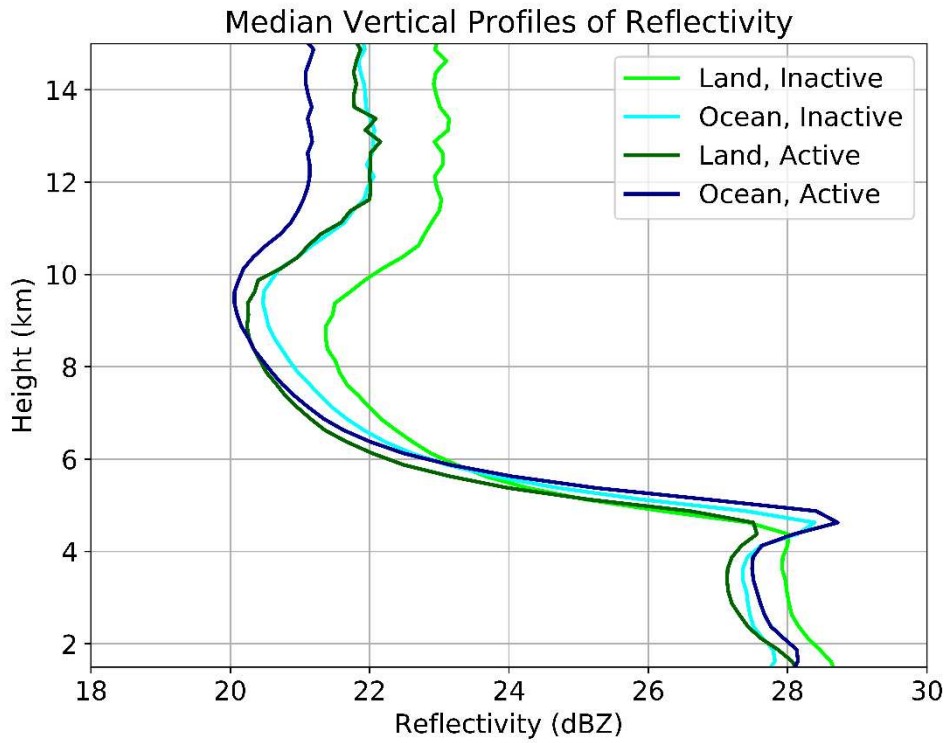

Figure 3.27: Median vertical profiles of reflectivity measured by TRMM PR and DPR KuPR over the land/ocean, and during inactive/active BSISO phases

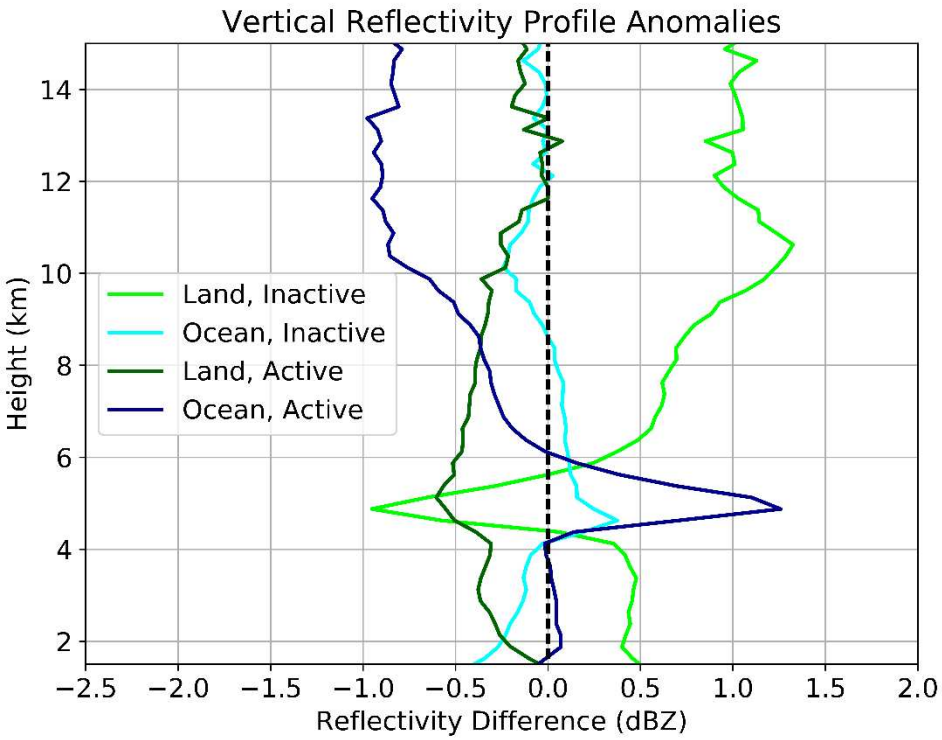

Figure 3.28: Vertical profiles of reflectivity anomalies, compared against a mean of all 4 profiles from Figure 3.27.

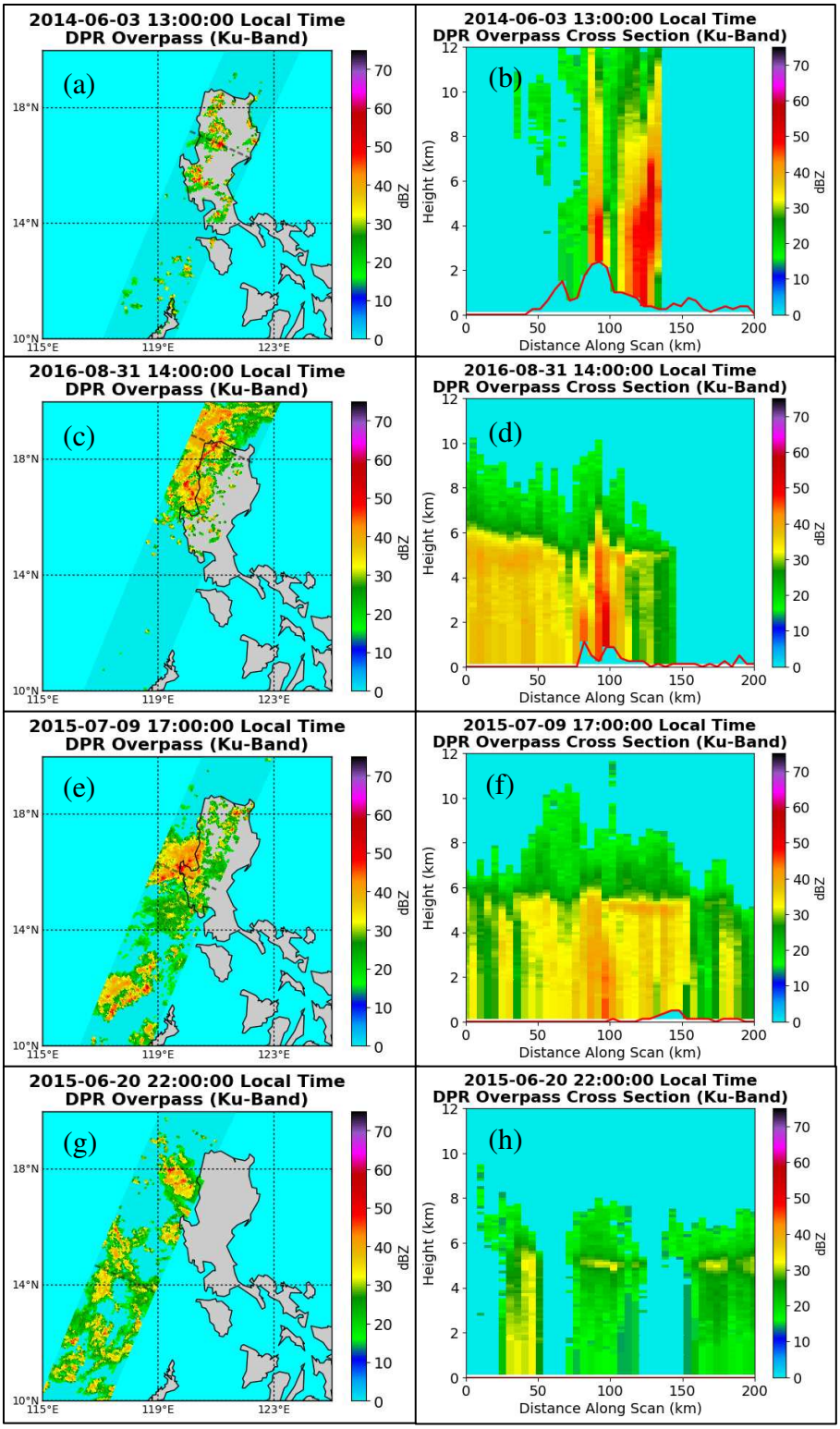

Figure 3.29: Individual DPR KuPR overpasses with composite reflectivity (a,c,e,g) and cross sections (b,d,f,h) during inactive (a,b,c,d) and active (e,f,g,h) BSISO phases. Dashed lines on the composite reflectivity plots represent where the cross section is taken through.

CHAPTER 4: DISCUSSION

The mechanisms proposed in previous studies for the off-shore rainfall maxima observed in the ASM region are reviewed here and discussed in the context of the results presented in the previous chapter. Modeling studies by Ogura and Yoshizaki (1998) suggested that wind shear and ocean surface heat fluxes were both required for off-shore precipitation. The results of this study also show this. During inactive phases, when ocean surface fluxes and deep vertical wind shear are reduced, due to the lack of a strong low-level monsoon flow, the amount of off-shore precipitation measured was also greatly reduced.

Precipitation occurs off the coast much more frequently in active periods, when the surface winds are stronger. When stratifying the data by wind regime rather than BSISO phase (Figure 3.9), this effect is even more clear. The westerly regime has strong low-level westerlies extending further north up the west coast of Luzon, and the precipitation signal follows this trend. Even in easterly wind regimes, there appears to be enhanced precipitation off the east coast. So, it seems clear that the low-level wind is a key to generating off-shore precipitation. The question remains as to what exactly is the mechanism that causes this.

One possibility is that the monsoon flow is interacting with the diurnal land/sea breeze cycle (Houze et al. 1981). At night, a local high pressure zone develops over the relatively cooler land. The resultant pressure gradient force is directed off-shore. This may create a land breeze which emanates outward and collides with the monsoon flow. Alternatively, even if a land breeze is not formed, the off-shore directed pressure gradient force would oppose the incoming monsoon winds, and would locally reduce their speed. Either of these would create convergence and lift needed to form precipitation. This theory is supported by Figure 3.13, which shows a strong diurnal

rotation in the coastal wind anomalies. This land breeze still exists in inactive phases, but the absence of a strong monsoon wind to converge may preclude the generation of precipitation.

Elevated terrain features are a common element to all of the regions that have these off-shore maxima (Wester Ghats, Myanmar, Luzon), and therefore seemingly play a role. The land/sea breeze theory, however, does not require these terrain features, so it likely does not tell the whole story. One readily apparent explanation may be orographic lift generated by the monsoon flow impinging on the mountains. However, because the rain maximum is just off the coast rather than directly over the mountains, this explanation also falls short.

In the NAME field project, convective cells would originate over land, and over time grow upscale and propagate off-shore, significantly contributing to rainfall there (Nesbitt et al. 1981; Lang et al. 2007). This mechanism requires there to be sufficient instability over the land in the daytime to generate the initial convection. Originally, it was believed that the increased cloud cover during active phases of the BSISO would hinder surface heating such that instability over the land would be too low to initiate convection. However, as shown in the previous chapter, there is still a notable diurnal cycle in land-based convection even during active phases. The reduction of instability over land may be partially compensated by increased orographic lifting from the impinging monsoon flow, or increased ocean surface fluxes. So off-shore propagation is still a viable explanation for the off-shore rainfall maximum seen in active phases. Indeed, an off-shore propagation signal is clear in the Hovmöller plot in Figure 3.19.

Although afternoon convection develops over the terrain during both inactive and active phases, the signal for off-shore propagation is much stronger in active phases. One explanation for this may be the reduction of wind shear during inactive phases. Vertical wind shear has widely been shown to be important to the development and maintenance of MCS's (Thorpe et al. 1982;

Moncrieff and Liu 1999; Coniglio et al. 2006; Zheng et al. 2013; Alfaro and Coniglio 2017). This was also found to be the case in both NAME (Lang et al. 2007) and TOGA-COARE (Saxen and Rutledge 2000). This also agrees with the modeling study of Ogura and Yoshizaki (1998), which showed that wind shear was necessary for off-shore precipitation. The addition of strong low-level winds during active BSISO phases and resulting enhancement of wind shear (particularly in the 700-100mb deep-layer), may be the extra component necessary to cause the afternoon terrain-based convection to organize upscale into an off-shore propagating MCS.

Xu et al. (2012) examined an extreme rain event on the island of Taiwan and proposed a mechanism for off-shore precipitation in which a cold pool generated from terrain-based convection spreads off-shore. The monsoon flow then converges with this cold pool barrier and is forced upward. In this mechanism the cold pool essentially acts as an extension of the elevated terrain. New precipitation is then generated at the convergence boundary between the low-level monsoon winds and the cold pool.

Another finding of the Xu et al. (2012) study was that convection persisted off-shore for an extended period of time (up to 12 hours). They hypothesized the island terrain was trapping the cold pool from spreading or moving away. Precipitation would be generated at the boundary between the cold pool and the low-level monsoon winds, where it would move in towards the island and gradually dissipate, which in turn would reinforce the cold pool. This positive feedback mechanism resulted in copious amounts of rain along and just off the coast. The persistent off-shore rainfall seen in all but the mid-afternoon hours in active phases could therefore be explained by the cold pool mechanism. The lack of convection over land during the evening and overnight hours may also be explained by this persistent, stable cold pool covering the land. The reduced off-shore precipitation during inactive phases can also be explained under this theory: the lack of

a low-level wind in inactive phases means that there is no convergence generated between the cold pool and the background flow. Therefore, little precipitation is generated, and the cold pool cannot be maintained.

Mapes et al. (2003) proposed a mechanism for off-shore precipitation in which daytime heating overland causes thermal expansion of the boundary layer. This perturbation is argued to create gravity waves, which then radiate outward over the ocean, destabilizing the atmosphere and driving convection (see the schematic in Figure 5.1, adapted from Mapes et al. 2003). The satellite and reanalysis data used in this study does not afford the temporal or spatial resolution needed to resolve mesoscale features like gravity waves. However, the presence of a diurnal cycle over Luzon, which was shown to occur during both inactive and active phases, suggests that the gravity wave theory is at least a possibility. In addition to daytime heating perturbing the boundary layer, strong, deep afternoon thunderstorms initiating over the terrain in Luzon (again, shown to occur in both inactive and active phases) may also generate gravity waves (Curry and Murty 1974; Dutta et al. 2009; Blanc et al. 2014).

This gravity wave mechanism, however, cannot account for why there appears to be a reduction in off-shore convection during inactive periods. In fact, during inactive periods when daytime heating is stronger (and the boundary layer thermal expansion more robust), one might expect there to be greater off-shore precipitation under this theory. The fact the opposite is true around Luzon during the summer months cast doubt on this gravity wave mechanism explaining the offshore precipitation west of Luzon. One possibility is that despite the gravity wave destabilization, the lower CAPE and reduced surface fluxes over the ocean preclude thunderstorm development.

CHAPTER 5: SUMMARY

The distinct rainfall maximum located off the western coast of Luzon during the ASM was examined in this study. Using high-resolution satellite radar data, surface wind measurements, and reanalysis of meteorological variables, precipitation intensity, morphology, amount, frequency, and location were all examined. The BSISO, a main driver of intraseasonal variability around Luzon, was shown to have significant impact on the amount of off-shore precipitation, in particular, west of Luzon. The presence of strong low-level monsoon south-westerlies during active phases of the BSISO, along with the associated increase in vertical wind shear and ocean surface heat flux, is thought to be the main contributor to increased off-shore precipitation observed at these times.

During inactive phases, Luzon frequently experiences afternoon deep convection with heavy rain and high lightning flash rates. Stratiform and rainfall over the SCS west of Luzon, however, are at a minimum during inactive phases. This agrees with previous work, where inactive phases were associated with reduced cloud cover, increased instability, and localized but intense thunderstorms over land (Ho et al. 2008; Xu and Zipser 2012). During active phases, however, large raining systems are frequent throughout the day, particularly over the ocean. While increased cloud coverage hinders surface heating and atmospheric stability, this is mitigated by the increase in ocean surface heat and moisture fluxes brought about by the strong southwest monsoon flow.

Previous field work (Mapes et al. 2003; Houze et al. 1981; Nesbitt et al. 2008; Xu et al. 2012; Ruppert et al. 2013) has shown that the diurnal cycle is a key component in creating off-shore precipitation. One of the key findings of this study is that a clear diurnal cycle in convection exists over the land during both inactive and active phases, despite the reduction in solar insolation

during the latter. During 15-21:00 local time, deep convection develops over the elevated terrain of west Luzon. This convection may then begin to grow upscale and propagate off-shore.

During inactive phases, the frequency of off-shore precipitation is much lower than in active phases. The low-level monsoon flow seems to be a critical component to generating this coastal rainfall. Proposed mechanisms by which this happens are as follows:

- At night, a localized high pressure zone develops over the relatively cool island. This sets up a pressure gradient force directed off-shore, which opposes the monsoon flow and creates convergence. This convergence and resulting lift support precipitation.
- The increase in low level winds increases the deep-layer (700-150 mb) wind shear, as well as the mid-level (850-500 mb) and low-level (surface – 850 mb) shear. This increase in shear (particularly deep-layer shear) is thought to be conducive to the development and maintenance of MCS's (Thorpe et al. 1982; Moncrieff and Liu 1999; Coniglio et al. 2006; Zheng et al. 2013; Alfaro and Coniglio 2017; Lang et al. 2007; Saxen and Rutledge 2000), which form as the afternoon convection over the mountains grows upscale and move westward. In inactive phases, absent of this wind shear, convective complexes struggle to survive long enough to propagate off-shore.
- A cold pool extending off the coast, which is generated by initial terrain-based convection and then pinned between the monsoon flow and the terrain, provides a boundary against which the low-level monsoon winds converge. This cold pool is then reinforced by rainfall generated by this convergence, and a positive-feedback cycle commences.

These theories are all supported by previous studies, and may indeed be working in tandem together. For example, while the off-shore propagation mechanism may explain the late-afternoon and evening coastal rainfall, the precipitation observed overnight may be better explained by the

land-breeze theory. The cold pool theory can cause precipitation for many hours on end (as seen in Xu et al. 2012) and could generate off-shore precipitation from late-afternoon through the night.

These mechanisms all involve mesoscale (or smaller) features which evolve on the order of hours. These processes cannot be resolved with satellite and reanalysis data alone. In order to fully resolve the details of the convergence boundaries and local wind features which are hypothesized here to be important, in-situ measurements with high spatio-temporal resolution are needed. This is the goal of the 2019 PISTON field campaign, which is proposed to take place off the west coast of Luzon. A shipborne dual-polarimetric weather radar (the CSU SEA-POL radar; Rutledge et al. 2019) will be used in conjunction with frequent balloon soundings and ocean profile measurements to analyze the land-sea-air interaction, and how it varies with the diurnal cycle.

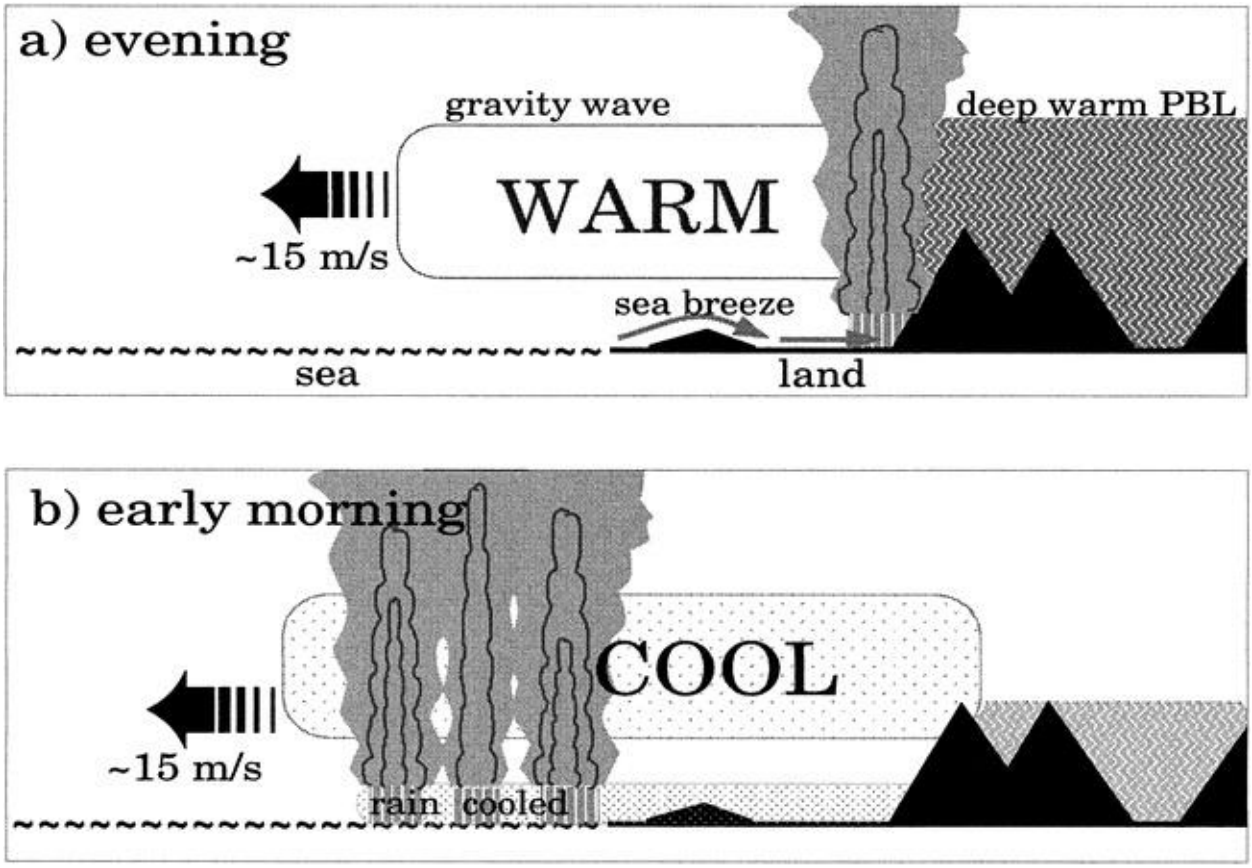

Figure 5.1: Schematic of a gravity wave propagating off-shore and generating convection. Adapted from Mapes et al. (2003).

REFERENCES

Alfaro, D. A., M. C. Coniglio, 2018: Discrimination of Mature and Dissipating Severe-Wind-Producing MCSs with Layer-Lifting Indices. Weather and Forecasting, 33, 3-21.

Atlas, R., R. N. Hoffman, J. Ardizzone, S. M. Leidner, J. C. Jusem, D. K. Smith, and D. Gombos, 2011: A cross-calibrated, multiplatform ocean surface wind velocity product for meteorological and oceanographic applications. Bull.Am.Meteorol.Soc., 92, 157-174.

Banzon, V., T. M. Smith, T. M. Chin, C. Liu, and W. Hankins, 2016: A long-term record of blended satellite and in situ sea-surface temperature for climate monitoring, modeling and environmental studies. Earth System Science Data, 8, 165-176.

Bjerknes, J., 1966: A possible response of the atmospheric Hadley circulation to equatorial anomalies of ocean temperature. Tellus, 18, 820-829.

Blanc, E., T. Farges, A. Le Pichon, and P. Heinrich, 2014: Ten year observations of gravity waves from thunderstorms in western Africa. Journal of Geophysical Research: Atmospheres, 119, 6409-6418.

Chang, C., Z. Wang, J. McBride, and C. Liu, 2005: Annual cycle of Southeast Asia—Maritime Continent rainfall and the asymmetric monsoon transition. J.Clim., 18, 287-301.

Chen, Y., P. Zhai, 2017: Simultaneous modulations of precipitation and temperature extremes in Southern parts of China by the boreal summer intraseasonal oscillation. Clim.Dyn., 49, 3363-3381.

Chow, K. C., J. C. Chan, 2009: Diurnal variations of circulation and precipitation in the vicinity of the Tibetan Plateau in early summer. Clim.Dyn., 32, 55-73.

Coniglio, M. C., D. J. Stensrud, and L. J. Wicker, 2006: Effects of upper-level shear on the structure and maintenance of strong quasi-linear mesoscale convective systems. J.Atmos.Sci., 63, 1231-1252.

Curry, M., R. Murty, 1974: Thunderstorm-generated gravity waves. J.Atmos.Sci., 31, 1402-1408.

Dai, A., K. E. Trenberth, 2004: The diurnal cycle and its depiction in the Community Climate System Model. J.Clim., 17, 930-951.

Dee, D. P., S. M. Uppala, A. Simmons, P. Berrisford, P. Poli, S. Kobayashi, U. Andrae, M. Balmaseda, G. Balsamo, and d. P. Bauer, 2011: The ERA-Interim reanalysis: Configuration and performance of the data assimilation system. Q.J.R.Meteorol.Soc., 137, 553-597.

Ding, Q., B. Wang, 2005: Circumglobal teleconnection in the Northern Hemisphere summer. J.Clim., 18, 3483-3505.

Ding, Q., B. Wang, 2009: Predicting extreme phases of the Indian summer monsoon. J.Clim., 22, 346-363.

Drushka, K., W. E. Asher, B. Ward, and K. Walesby, 2016: Understanding the formation and evolution of rain-formed fresh lenses at the ocean surface. Journal of Geophysical Research: Oceans, 121, 2673-2689.

Dutta, G., A. Kumar, P. Vinay Kumar, M. Venkat Ratnam, M. Chandrashekar, Y. Shibagaki, M. Salauddin, and H. Basha, 2009: Characteristics of high-frequency gravity waves generated by tropical deep convection: Case studies. Journal of Geophysical Research: Atmospheres, 114.

Emanuel, K. A., 1986: An air-sea interaction theory for tropical cyclones. Part I: Steady-state maintenance. J.Atmos.Sci., 43, 585-605.

Fasullo, J., P. Webster, 2003: A hydrological definition of Indian monsoon onset and withdrawal. J.Clim., 16, 3200-3211.

Flohn, H., 1957: Large-scale aspects of the "summer monsoon" in South and East Asia. Journal of the Meteorological Society of Japan.Ser.II, 35, 180-186.

Fore, A. G., B. W. Stiles, A. H. Chau, B. A. Williams, R. S. Dunbar, and E. Rodríguez, 2014: Point-wise wind retrieval and ambiguity removal improvements for the QuikSCAT climatological data set. IEEE Trans.Geosci.Remote Sens., 52, 51-59.

Fu, C., J. O. Fletcher, 1985: The relationship between Tibet-tropical ocean thermal contrast and interannual variability of Indian monsoon rainfall. Journal of climate and applied meteorology, 24, 841-847.

Fu, X., B. Wang, D. E. Waliser, and L. Tao, 2007: Impact of atmosphere–ocean coupling on the predictability of monsoon intraseasonal oscillations. J.Atmos.Sci., 64, 157-174.

Gille, S. T., S. G. Llewellyn Smith, and N. M. Statom, 2005: Global observations of the land breeze. Geophys.Res.Lett., 32.

Grossman, R. L., D. R. Durran, 1984: Interaction of low-level flow with the western Ghat Mountains and offshore convection in the summer monsoon. Mon.Weather Rev., 112, 652-672.

He, H., J. W. McGinnis, Z. Song, and M. Yanai, 1987: Onset of the Asian summer monsoon in 1979 and the effect of the Tibetan Plateau. Mon.Weather Rev., 115, 1966-1995.

Ho, C., M. Park, Y. Choi, and Y. N. Takayabu, 2008: Relationship between intraseasonal oscillation and diurnal variation of summer rainfall over the South China Sea. Geophys.Res.Lett., 35.

Houze Jr, R. A., S. G. Geotis, F. D. Marks Jr, and A. K. West, 1981: Winter monsoon convection in the vicinity of north Borneo. Part I: Structure and time variation of the clouds and precipitation. Mon.Weather Rev., 109, 1595-1614.

Hoyos, C. D., P. J. Webster, 2007: The role of intraseasonal variability in the nature of Asian monsoon precipitation. J.Clim., 20, 4402-4424.

Hsu, P., J. Lee, and K. Ha, 2016: Influence of boreal summer intraseasonal oscillation on rainfall extremes in southern China. Int.J.Climatol., 36, 1403-1412.

Huang, R., W. Li, 1988: Influence of heat source anomaly over the western tropical Pacific on the subtropical high over East Asia and its physical mechanism. Chinese J.Atmos.Sci, 12, 107-116.

Johnson, R. H., T. M. Rickenbach, S. A. Rutledge, P. E. Ciesielski, and W. H. Schubert, 1999: Trimodal characteristics of tropical convection. J.Clim., 12, 2397-2418.

Kang, I., C. Ho, Y. Lim, and K. Lau, 1999: Principal modes of climatological seasonal and intraseasonal variations of the Asian summer monsoon. Mon.Weather Rev., 127, 322-340.

Kemball-Cook, S., B. Wang, 2001: Equatorial waves and air–sea interaction in the boreal summer intraseasonal oscillation. J.Clim., 14, 2923-2942.

Kim, H., I. Kang, 2008: The impact of ocean–atmosphere coupling on the predictability of boreal summer intraseasonal oscillation. Clim.Dyn., 31, 859.

Kripalani, R., A. Kulkarni, 1997: Rainfall variability over South–east Asia—connections with Indian monsoon and ENSO extremes: new perspectives. Int.J.Climatol., 17, 1155-1168.

Kripalani, R., A. Kulkarni, 2001: Monsoon rainfall variations and teleconnections over South and East Asia. Int.J.Climatol., 21, 603-616.

Krishnamurti, T., S. Cocke, R. Pasch, and S. Low-Nam, 1983: Precipitation estimates from raingauge and satellite observations, summer MONEX. FSU report, 83.

Kummerow, C., W. Barnes, T. Kozu, J. Shiue, and J. Simpson, 1998: The tropical rainfall measuring mission (TRMM) sensor package. J.Atmos.Ocean.Technol., 15, 809-817.

Lang, T. J., D. A. Ahijevych, S. W. Nesbitt, R. E. Carbone, S. A. Rutledge, and R. Cifelli, 2007: Radar-observed characteristics of precipitating systems during NAME 2004. J.Clim., 20, 1713-1733.

Lau, K., P. Chan, 1986: Aspects of the 40–50 day oscillation during the northern summer as inferred from outgoing longwave radiation. Mon.Weather Rev., 114, 1354-1367.

Lau, K., C. Sui, 1997: Mechanisms of short-term sea surface temperature regulation: Observations during TOGA COARE. J.Clim., 10, 465-472.

Lau, K., K. Kim, 2006: Observational relationships between aerosol and Asian monsoon rainfall, and circulation. Geophys.Res.Lett., 33.

Lau, K., H. Wu, 2001: Principal modes of rainfall–SST variability of the Asian summer monsoon: A reassessment of the monsoon–ENSO relationship. J.Clim., 14, 2880-2895.

Lee, J., B. Wang, M. C. Wheeler, X. Fu, D. E. Waliser, and I. Kang, 2013: Real-time multivariate indices for the boreal summer intraseasonal oscillation over the Asian summer monsoon region. Clim.Dyn., 40, 493-509.

Lee, S., J. Moon, B. Wang, and H. Kim, 2017: Subseasonal Prediction of Extreme Precipitation over Asia: Boreal Summer Intraseasonal Oscillation Perspective. J.Clim., 30, 2849-2865.

Li, C., M. Yanai, 1996: The onset and interannual variability of the Asian summer monsoon in relation to land–sea thermal contrast. J.Clim., 9, 358-375.

Lin, J., G. N. Kiladis, B. E. Mapes, K. M. Weickmann, K. R. Sperber, W. Lin, M. C. Wheeler, S. D. Schubert, A. Del Genio, and L. J. Donner, 2006: Tropical intraseasonal variability in 14 IPCC AR4 climate models. Part I: Convective signals. J.Clim., 19, 2665-2690.

Liu, C., E. J. Zipser, D. J. Cecil, S. W. Nesbitt, and S. Sherwood, 2008: A cloud and precipitation feature database from nine years of TRMM observations. Journal of Applied Meteorology and Climatology, 47, 2712-2728.

Maloney, E. D., S. K. Esbensen, 2005: A modeling study of summertime east Pacific wind-induced ocean–atmosphere exchange in the intraseasonal oscillation. J.Clim., 18, 568-584.

Mapes, B. E., T. T. Warner, and M. Xu, 2003: Diurnal patterns of rainfall in northwestern South America. Part III: Diurnal gravity waves and nocturnal convection offshore. Mon.Weather Rev., 131, 830-844.

Matsueda, M., H. Endo, 2011: Verification of medium-range MJO forecasts with TIGGE. Geophys.Res.Lett., 38.

Mohr, K. I., E. J. Zipser, 1996: Mesoscale convective systems defined by their 85-GHz ice scattering signature: Size and intensity comparison over tropical oceans and continents. Mon.Weather Rev., 124, 2417-2437.

Moncrieff, M. W., C. Liu, 1999: Convection initiation by density currents: Role of convergence, shear, and dynamical organization. Mon.Weather Rev., 127, 2455-2464.

Nesbitt, S. W., D. J. Gochis, and T. J. Lang, 2008: The diurnal cycle of clouds and precipitation along the Sierra Madre Occidental observed during NAME-2004: Implications for warm season precipitation estimation in complex terrain. J.Hydrometeorol., 9, 728-743.

Nitta, T., 1987: Convective activities in the tropical western Pacific and their impact on the Northern Hemisphere summer circulation. Journal of the Meteorological Society of Japan.Ser.II, 65, 373-390.

Ogura, Y., M. Yoshizaki, 1988: Numerical study of orographic-convective precipitation over the eastern Arabian Sea and the Ghat Mountains during the summer monsoon. J.Atmos.Sci., 45, 2097-2122.

Petersen, W. A., S. A. Rutledge, 2001: Regional variability in tropical convection: Observations from TRMM. J.Clim., 14, 3566-3586.

Petersen, W. A., S. A. Rutledge, and R. E. Orville, 1996: Cloud-to-ground lightning observations from TOGA COARE: Selected results and lightning location algorithms. Mon.Weather Rev., 124, 602-620.

Pillai, P. A., H. Annamalai, 2012: Moist dynamics of severe monsoons over South Asia: Role of the tropical SST. J.Atmos.Sci., 69, 97-115.

Rosenfeld, D., I. M. Lensky, 1998: Satellite-based insights into precipitation formation processes in continental and maritime convective clouds. Bull.Am.Meteorol.Soc., 79, 2457-2476.

Rotunno, R., J. B. Klemp, and M. L. Weisman, 1988: A theory for strong, long-lived squall lines. J.Atmos.Sci., 45, 463-485.

Ruppert Jr, J. H., R. H. Johnson, and A. K. Rowe, 2013: Diurnal circulations and rainfall in Taiwan during SoWMEX/TiMREX (2008). Mon.Weather Rev., 141, 3851-3872.

Sabeerali, C., A. Ramu Dandi, A. Dhakate, K. Salunke, S. Mahapatra, and S. A. Rao, 2013: Simulation of boreal summer intraseasonal oscillations in the latest CMIP5 coupled GCMs. Journal of Geophysical Research: Atmospheres, 118, 4401-4420.

Saxen, T. R., S. A. Rutledge, 2000: Surface rainfall–cold cloud fractional coverage relationship in TOGA COARE: A function of vertical wind shear. Mon.Weather Rev., 128, 407-415.

Singh, P., K. Nakamura, 2009: Diurnal variation in summer precipitation over the central Tibetan Plateau. Journal of Geophysical Research: Atmospheres, 114.

Smith, R. B., 1980: Linear theory of stratified hydrostatic flow past an isolated mountain. Tellus, 32, 348-364.

Thorpe, A., M. Miller, and M. Moncrieff, 1982: Two-dimensional convection in non-constant shear: A model of mid-latitude squall lines. Q.J.R.Meteorol.Soc., 108, 739-762.

Turner, A. G., H. Annamalai, 2012: Climate change and the South Asian summer monsoon. Nature Climate Change, 2, 587.

Virts, K. S., R. A. Houze Jr, 2016: Seasonal and intraseasonal variability of mesoscale convective systems over the South Asian Monsoon Region. J.Atmos.Sci., 73, 4753-4774

Waliser, D., K. Jin, I. Kang, W. Stern, S. Schubert, M. Wu, K. Lau, M. Lee, V. Krishnamurthy, and A. Kitoh, 2003: AGCM simulations of intraseasonal variability associated with the Asian summer monsoon. Clim.Dyn., 21, 423-446.

Wang, B., Y. Ding, 1992: An overview of the Madden-Julian oscillation and its relation to monsoon and mid-latitude circulation. Adv.Atmos.Sci., 9, 93-111.

Wang, B., H. Rui, 1990: Synoptic climatology of transient tropical intraseasonal convection anomalies: 1975–1985. Meteorology and Atmospheric Physics, 44, 43-61.

Wang, B., R. Wu, and K. Lau, 2001: Interannual variability of the Asian summer monsoon: Contrasts between the Indian and the western North Pacific–East Asian monsoons. J.Clim., 14, 4073-4090.

Wang, B., X. Xie, 1997: A model for the boreal summer intraseasonal oscillation. J.Atmos.Sci., 54, 72-86.

Wang, J., L. D. Carey, 2005: The development and structure of an oceanic squall-line system during the South China Sea Monsoon Experiment. Mon.Weather Rev., 133, 1544-1561.

Wang, Y., W. Tao, and J. Simpson, 1996: The impact of ocean surface fluxes on a TOGA COARE convective system. Mon.Weather Rev., 124, 2753-2763.

Wang, Z., C. Chang, 2012: A numerical study of the interaction between the large-scale monsoon circulation and orographic precipitation over South and Southeast Asia. J.Clim., 25, 2440-2455.

Wheeler, M. C., H. H. Hendon, 2004: An all-season real-time multivariate MJO index: Development of an index for monitoring and prediction. Mon.Weather Rev., 132, 1917-1932.

Wijesekera, H., C. Paulson, and A. Huyer, 1999: The effect of rainfall on the surface layer during a westerly wind burst in the western equatorial Pacific. J.Phys.Oceanogr., 29, 612-632.

Williams, E., S. Stanfill, 2002: The physical origin of the land–ocean contrast in lightning activity. Comptes Rendus Physique, 3, 1277-1292.

Williams, E. R., S. Geotis, N. Renno, S. Rutledge, E. Rasmussen, and T. Rickenbach, 1992: A radar and electrical study of tropical "hot towers". J.Atmos.Sci., 49, 1386-1395.

Xie, S., H. Xu, N. Saji, Y. Wang, and W. T. Liu, 2006: Role of narrow mountains in large-scale organization of Asian monsoon convection. J.Clim., 19, 3420-3429.

Xu, W., S. A. Rutledge, 2018: Convective Variability associated with the Boreal Summer Intraseasonal Oscillation in the South China Sea Region. J.Clim., 31, 7363-7383.

Xu, W., E. J. Zipser, 2012: Properties of deep convection in tropical continental, monsoon, and oceanic rainfall regimes. Geophys.Res.Lett., 39.

Xu, W., E. J. Zipser, Y. Chen, C. Liu, Y. Liou, W. Lee, and B. Jong-Dao Jou, 2012: An orography-associated extreme rainfall event during TiMREX: Initiation, storm evolution, and maintenance. Mon.Weather Rev., 140, 2555-2574.

Yang, G., J. Slingo, 2001: The diurnal cycle in the tropics. Mon.Weather Rev., 129, 784-801.

Ding, Y., J. C. Chan, 2005: The East Asian summer monsoon: an overview. Meteorology and Atmospheric Physics, 89, 117-142.

Zheng, L., J. Sun, X. Zhang, and C. Liu, 2013: Organizational modes of mesoscale convective systems over central East China. Weather and Forecasting, 28, 1081-1098.

Zipser, E. J., K. R. Lutz, 1994: The vertical profile of radar reflectivity of convective cells: A strong indicator of storm intensity and lightning probability? Mon.Weather Rev., 122, 1751-1759.

Zuidema, P., 2003: Convective clouds over the Bay of Bengal. Mon.Weather Rev., 131, 780-798.